Supplementary Materials: Visible Light-Induced Homolytic Cleavage of Perfluoroalkyl Iodides Mediated by Phosphines

Mario Bracker [1], Lucas Helmecke [2], Martin Kleinschmidt [1]*, Constantin Czekelius [2]* and Christel M. Marian [1]*

March 30, 2020

Contents

S1. General Experimental Procedures

All preparations involving air- and moisture-sensitive compounds were carried out inside a glove box (*Vacuum Atmospheres* model OMNI-LAB) under N_2 atmosphere (*Air Liquide ALPHAGAZ*™ 5.0). Glassware was dried for 2 hours at 120 °C and cooled down in vacuo.

Nonafluoro-1-iodobutane was purchased from TCI and was filtered through a column packed with aluminum oxide 90 basic 0.063 - 0.200 mm (activity stage I) and activated molecular sieve (4 Å) under N_2 atmosphere. The clear and colorless liquid was stored in amber glass vials under N_2 atmosphere. Tri-*tert*-butylphosphine was purchased from Sigma Aldrich.

Pentane and dichloromethane were dried with the solvent purification system MP-SPS 800 from M.Braun and degassed with freeze-pump-thaw.

^{1}H-, ^{13}C, ^{31}P-spectra were recorded on *Bruker* Avance III 300 and 600. Chemical shifts are reported in parts per million (ppm) to the corresponding solvent. The order of citation in parentheses is a) multiplicity (s = singlet, d = doublet, m = multiplet), b) coupling constants, c) number of protons, and d) assignment. Coupling constants (J) were reported in Hertz (Hz). If not described differently, the NMR-spectra were measured at 298 K.

UV-VIS spectra were measured on a Perkin Elmer Lamda 2 UV-VIS spectrometer in Hellma cuvettes (10 x 10 mm, Suprasil quartz glass).

GC measurements were performed on a Shimadzu GC-2010 equipped with an auto injector AOC-20i (syringe code: 10R-S-0.63C). A ZB-Wax Plus column (30 × 0.25 mm × 0.25 μm) was used. As internal standard *n*-decane (Acros Organics, purity 99 + %, LOT:1283567) was added to the reaction solution. The used photoreactor is self-assembled and is described in literature. [1]

S2. Synthesis of phosphites

S2.1. 4-Methyl-2,6,7-trioxa-1-phosphabicyclo-[2,2,2]-octane (caged phosphite)

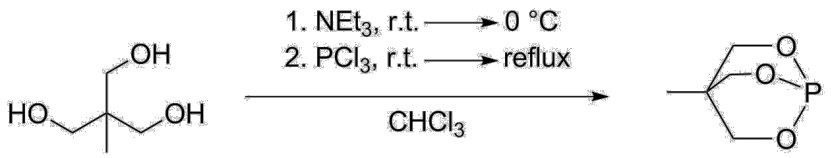

The synthesis of 4-methyl-2,6,7-trioxa-1-phosphabicyclo-[2,2,2]-octane was conducted similar to a literature known procedure. [2] In a 250 ml two-necked round-bottom flask with condenser tris(hydroxymethyl)ethane (7.21 g, 60.0 mmol, 1.0 equiv) and triethylamine (19.2 ml, 138 mmol, 2.3 equiv) were dissolved in $CHCl_3$ (70 ml). PCl_3 (5.2 ml, 59 mmol) in $CHCl_3$ (10 ml) was added dropwise at 0 °C to the cloudy reaction solution. After removing the ice bath the reaction solution was clear and was refluxed for 12 h. The clear reaction solution was extracted with desalinated water (3 × 50 ml), dried over anhydrous $MgSO_4$, filtered and the solvent was evaporated. The obtained colorless gel-like crystals were dissolved in CH_2Cl_2 (4 ml) and the solvent was evaporated again yielding colorless crystals.

yield (148.1 g mol^{-1}) 4.70 g (31.7 mmol, 53%)

^{1}H-NMR (600 MHz, $CDCl_3$) δ [ppm] 3.94 (d, J = 1.9 Hz, CH_2, 6H), 0.73 (s, CH_3, 3H)

^{13}C-NMR (75.5 MHz, $CDCl_3$) δ [ppm] 71.94 (s, C—CH_3), 32.13 (d, J = 22.5 Hz, CH_2), 16.82 (d, J = 5.5 Hz, CH_3)

^{31}P-NMR (243 MHz, $CDCl_3$) δ [ppm] 91.2

Mp: 91.2 – 96.9 °C

Analytic data are consistent with literature-known values. [2,3]

*S2.2. Tri-*tert*-butyl phosphite*

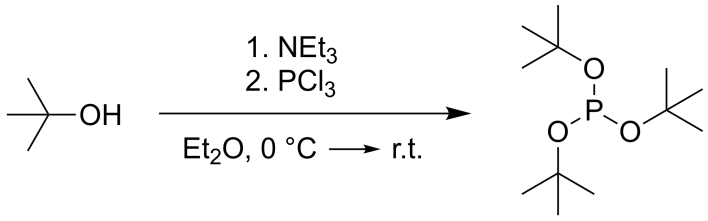

The synthesis of tri-*tert*-butyl phosphite was conducted similar to a literature known procedure. [4] Anhydrous diethyl ether was degassed with freeze-pump-thaw and each educt was degassed in Et_2O again before it was added. *Tert*-butyl alcohol (11.7 ml, 0.125 mol, 2.94 equiv) in Et_2O (25 ml) and triethylamine (17.3 ml, 0.125 mol, 2.94 equiv) in Et_2O (25 ml) were added together at 0 °C. PCl_3 (3.70 ml, 0.0425 mol) in Et_2O (12 ml) was added slowly via a dropping funnel, so that the reaction temperature maintained between 0 °C and 5 °C. After the addition was completed, Et_2O (30 ml) was added to the reaction solution and the reaction mixture was stirred 1 h at 0 °C and 16 h at r.t.. The reaction solution was separated via Schlenk filtration and the solvent was removed in vacuo. While the solvent was removed the round-bottom flask was cooled with an ice/water bath. A pale yellow oil was obtained, transferred into the glovebox and filtered through a syringe filter.

yield (250.3 g mol^{-1}) 871.6 mg (3.48 mmol, 8%)

^{1}H-NMR (300 MHz, C_6D_6) δ [ppm] 1.39 (s, (CH_3)$_3$C).

^{13}C-NMR (75.5 MHz, C_6D_6) δ [ppm] 76.1 (s, $(CH_3)_3C$), 31.4 (s, $(CH_3)_3C$)

^{31}P-NMR (121 MHz, C_6D_6) δ [ppm] 151.1

^{1}H-NMR (300 MHz, $CDCl_3$) δ [ppm] 1.28 (s, (CH_3)$_3$C).

^{13}C-NMR (75.5 MHz, $CDCl_3$) δ [ppm] 75.8 (d, J = 6.0 Hz, $(CH_3)_3C$), 31.1 (d, J = 8.1 Hz, $(CH_3)_3C$)

^{31}P-NMR (121 MHz, $CDCl_3$) δ [ppm] 140.1

Analytic data are consistent with literature-known values. [4–6]

S3. Reactions

S3.1. Reaction with 4-methyl-2,6,7-trioxa-1-phosphabicyclo-[2,2,2]-octane (caged phosphite)

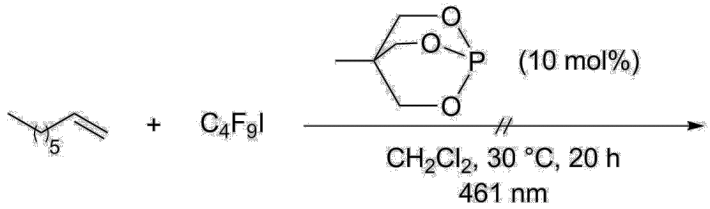

Caged phosphite (8.0 mg, 0.054 mmol, 10 mol%) was weighed into a 4 ml screw neck glass vial. Under a stream of nitrogen 1-octene (84 μl, 0.530 mmol) and CH_2Cl_2 (2 ml) were added. Under red light and the stream of nitrogen C_4F_9I (100 μl, 0.583 mmol, 1.10 equiv) was added, the vial was sealed with a septa screw cap and the reaction solution was irradiated (461 nm) for 20 h. After 1 h, 4 h and 20 h samples for a control by NMR spectroscopy were withdrawn under a stream of nitrogen and under red light. No conversion was observed.

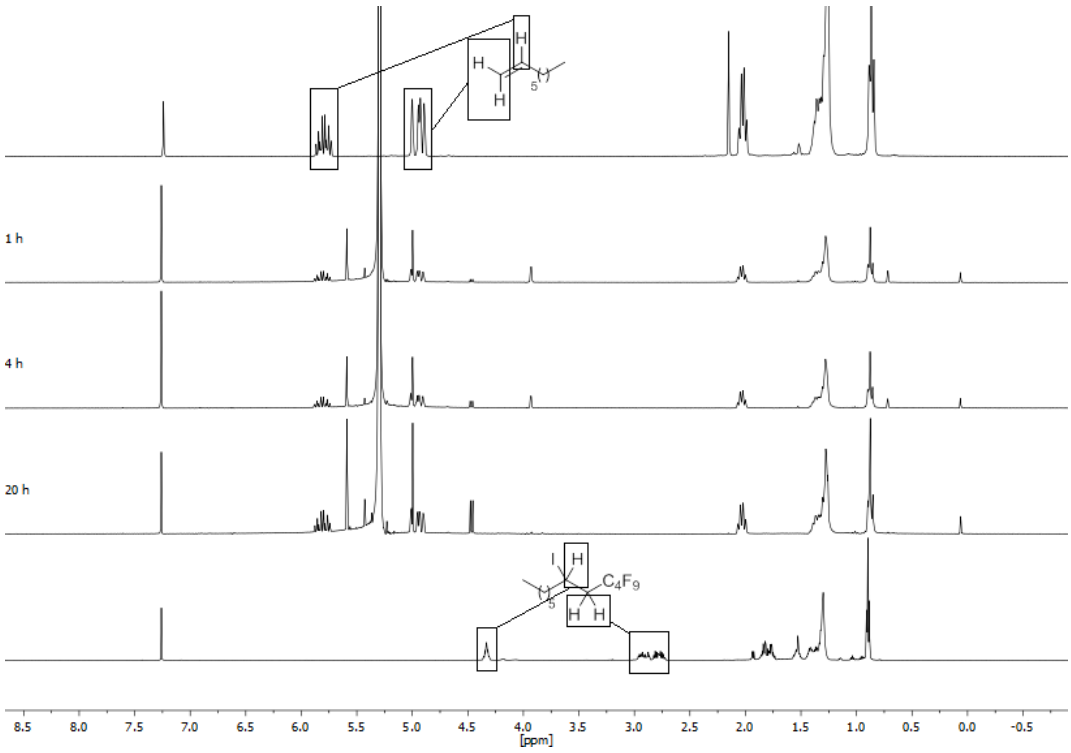

^{1}H-NMR-spectra (300 MHz, $CDCl_3$) of the reaction after 1 h, 4 h and 20 h in comparison with spectra of 1-octene (top) and the iodo perfluoroalkylation products (bottom).

*S3.2. Reaction with tri-*tert*-butylphosphite*

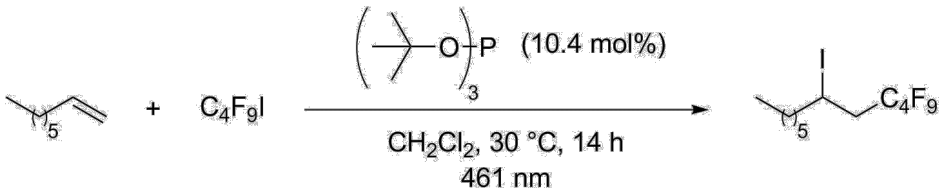

Inside the glovebox tri-*tert*-butylphoshite (14.4 mg, 0.0575 mmol, 10.4 mol%), *n*-decane (29.6 mg) and 1-octene (62.0 mg, 0.552 mmol) were weighed into a 4 ml screw neck glass vial. A Teflon stirring bar and CH_2Cl_2 (2 ml) were added. Under red light C_4F_9I (100 μl, 0.583 mmol, 1.05 equiv) was added, the vial was sealed with a septa screw cap and the reaction solution was irradiated (461 nm) for 14 h. After 1 h (conversion: 31%), 2 h (conversion: 51%) and 14 h (conversion: 56%) samples for a reaction control by GC were withdrawn under a stream of nitrogen. With a 1.0 ml syringe (Braun) flushed with N_2 0.10 ml of the reaction solution were withdrawn and diluted with 0.4 ml CH_2Cl_2 in a short amber thread vial. The vial was sealed with a black screw cap.

S4. NMR Spectra

S4.1. Caged phosphite

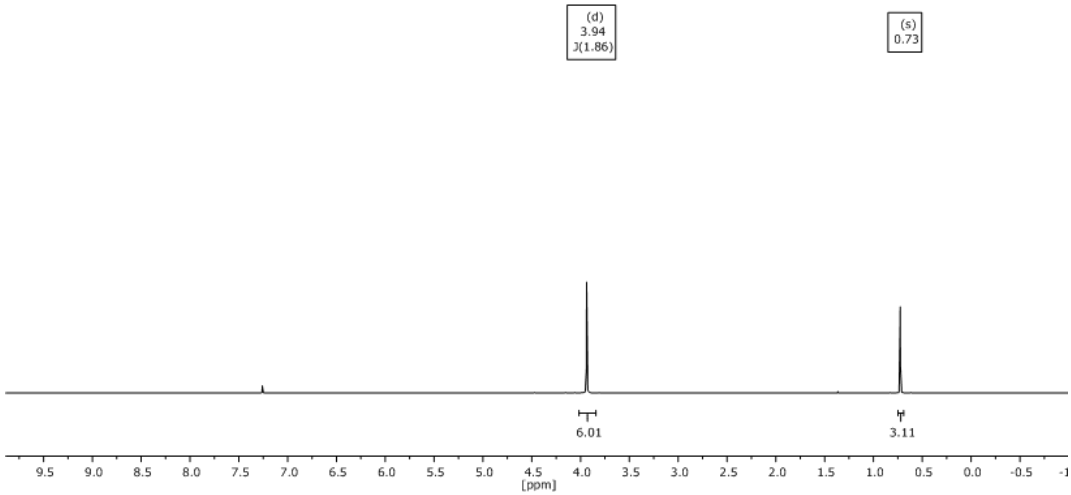

^{1}H-NMR-spectrum (600 MHz. $CDCl_3$)

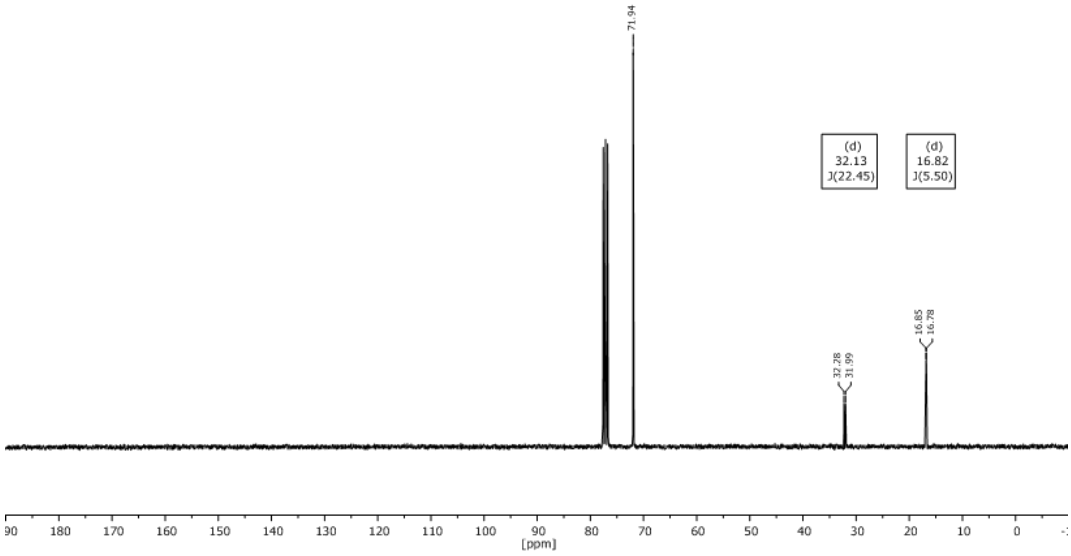

^{13}C-NMR-spectrum (75.5 MHz. $CDCl_3$)

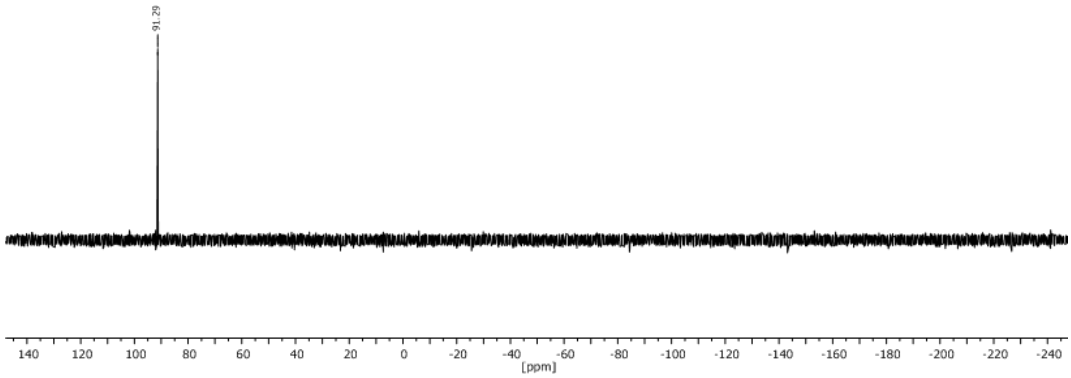

^{31}P-NMR-spectrum (243 MHz. $CDCl_3$)

S4.2. (^{t}BuO)$_3$P

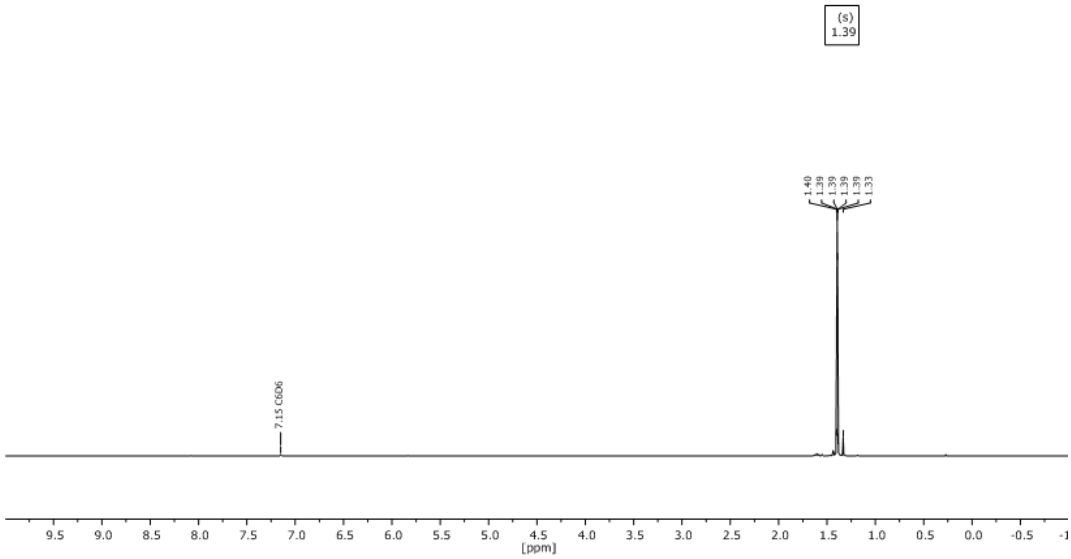

^{1}H-NMR-spectrum (300 MHz. C_6D_6)

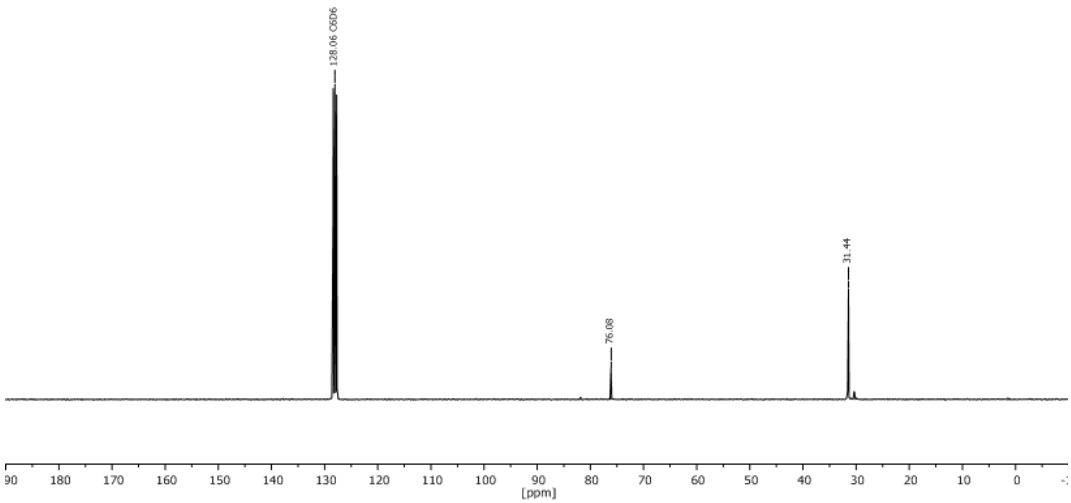

^{13}C-NMR-spectrum (75.5 MHz. C_6D_6)

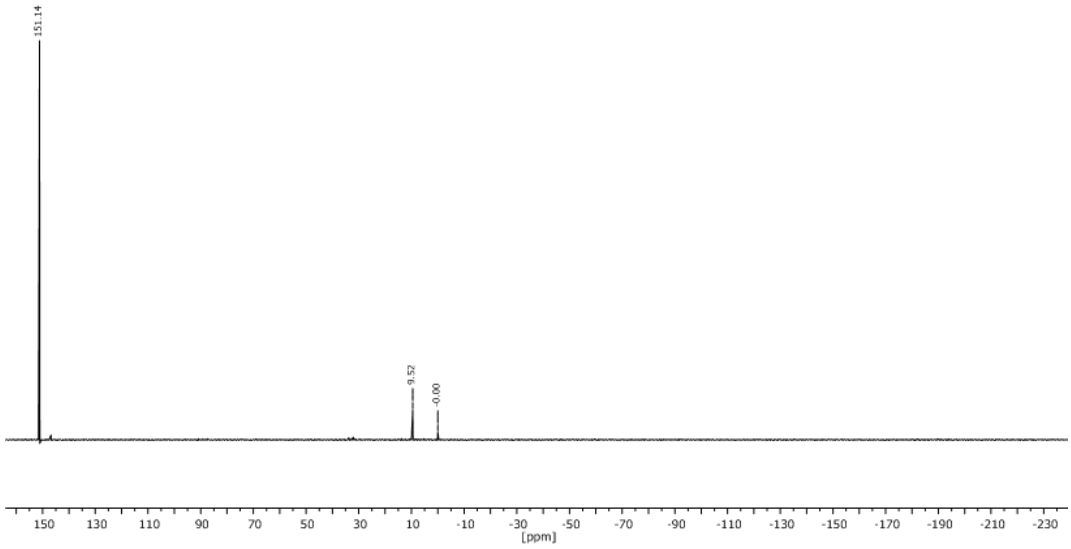

^{31}P-NMR-spectrum (121 MHz. $CDCl_3$)

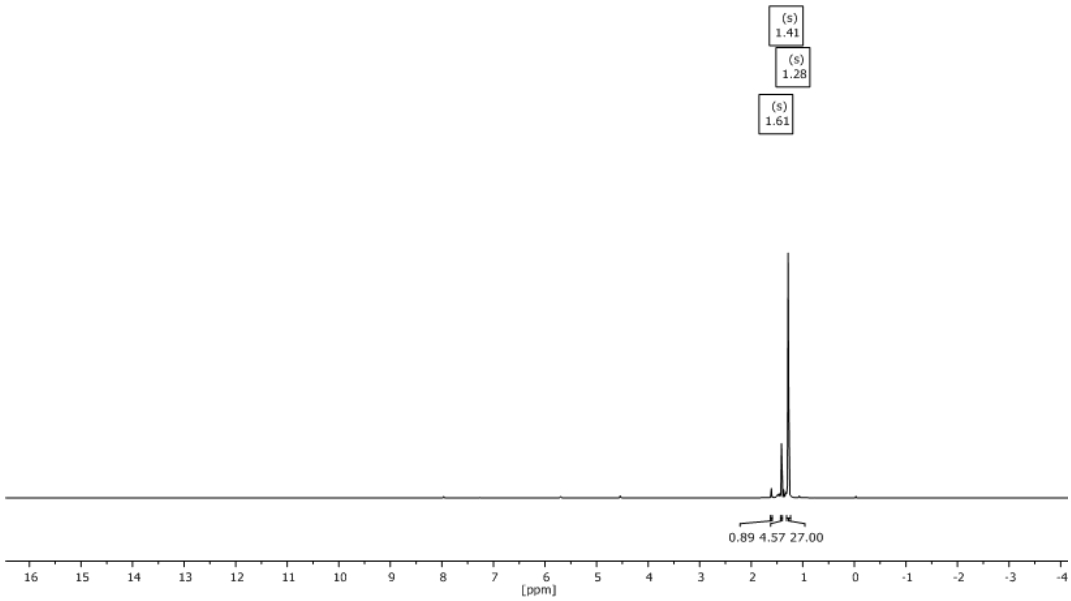

^{1}H-NMR-spectrum (300 MHz. $CDCl_3$)

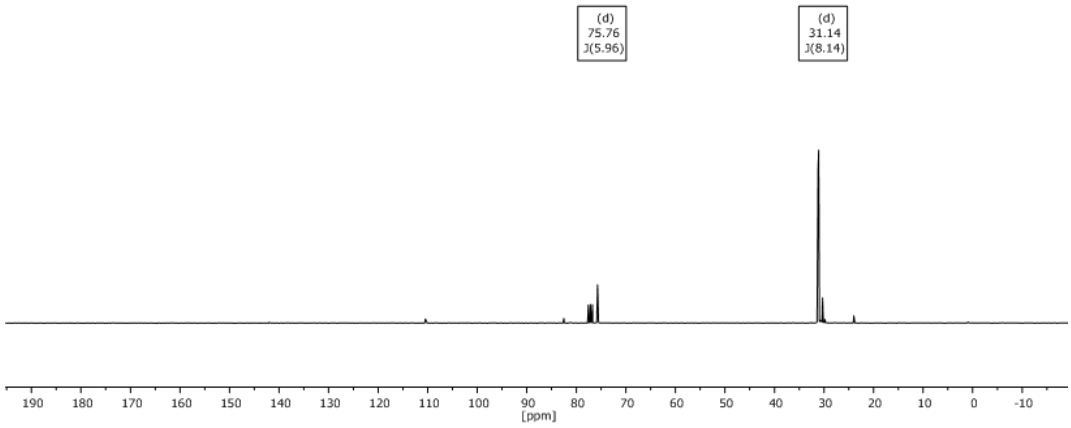

^{13}C-NMR-spectrum (75.5 MHz. $CDCl_3$)

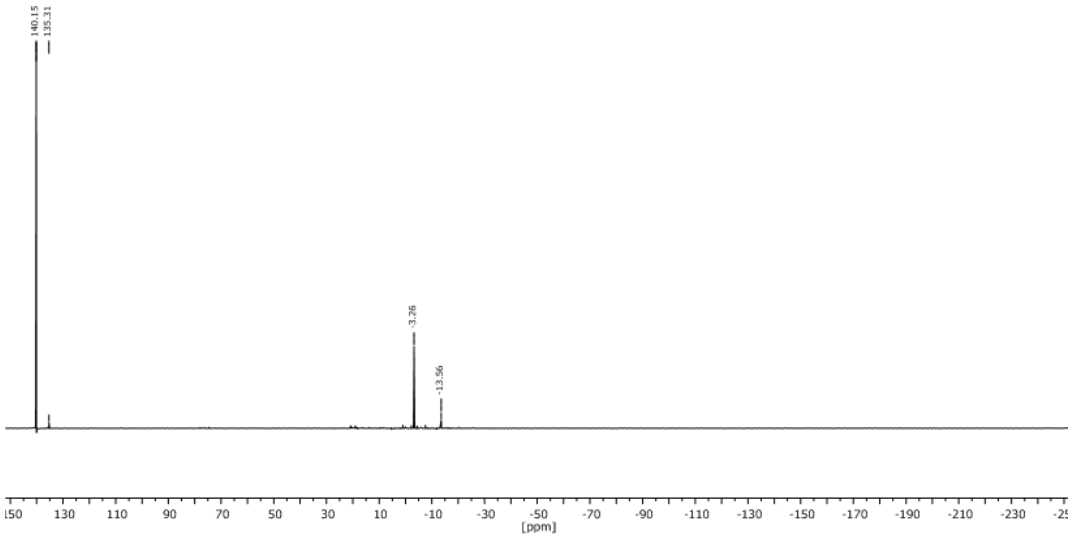

^{31}P-NMR-spectrum (121 MHz. $CDCl_3$)

S5. UV-Vis Measurements

- C_4F_9I (34.6 mg, 0.100 mmol) was dissolved in pentane or CH_2Cl_2 (10.0 ml) inside the glovebox in a volumetric flask. This solution was diluted in a volumetric flask (200 μL in 2.00 ml). The following concentration was present: [C_4F_9I] = 1.0 mM.
- ^{t}Bu$_3$P (20.2 mg, 0.100 mmol) was dissolved in pentane or CH_2Cl_2 (10.0 ml) in a volumetric flask inside the glovebox. This solution was diluted in a volumetric flask (200 μL in 2.00 ml). The following concentration was present: [^{t}Bu$_3$P] = 1 mM.
- ^{t}Bu$_3$P (20.2 mg, 0.100 mmol) and C_4F_9I (34.6 mg, 0.100 mmol) were dissolved in pentane or CH_2Cl_2 (10.0 ml) in a volumetric flask inside the glovebox. This solution was diluted in a volumetric flask (200 μL in 2.00 ml). The following concentration was present: [^{t}Bu$_3$P] = 1 mM, [C_4F_9I] = 1 mM.
- caged phosphine (14.8 mg, 0.100 mmol) was dissolved in CH_2Cl_2 (10.0 ml) in a volumetric flask. This solution was diluted in a volumetric flask (200 μL in 2.00 ml). The following concentration was present: [caged phosphine] = 1.0 mM.
- caged phosphine (14.8 mg, 0.100 mmol) and C_4F_9I (34.6 mg, 0.100 mmol) were dissolved in CH_2Cl_2 (10.0 ml) in a volumetric flask. This solution was diluted in a volumetric flask (200 μL in 2.00 ml). The following concentration was present: [caged phosphine] = 1 mM, [C_4F_9I] = 1 mM.
- (MeO)$_3$P (12.4 mg, 0.100 mmol) was dissolved in CH_2Cl_2 (10.0 ml) in a volumetric flask. This solution was diluted in a volumetric flask (200 μL in 2.00 ml). The following concentration was present: [(MeO)$_3$P] = 1.0 mM.
- (MeO)$_3$P (12.4 mg, 0.100 mmol) and C_4F_9I (34.6 mg, 0.100 mmol) were dissolved in CH_2Cl_2 (10.0 ml) in a volumetric flask. This solution was diluted in a volumetric flask (200 μL in 2.00 ml). The following concentration was present: [(MeO)$_3$P] = 1 mM, [C_4F_9I] = 1 mM.
- (^{t}BuO)$_3$P (25.2 mg, 0.100 mmol) was dissolved in CH_2Cl_2 (10.0 ml) inside the glovebox in a volumetric flask. This solution was diluted in a volumetric flask (200 μL in 2.00 ml). The following concentration was present: [(^{t}BuO)$_3$P] = 1.0 mM.
- (^{t}BuO)$_3$P (25.2 mg, 0.100 mmol) and C_4F_9I (34.6 mg, 0.100 mmol) were dissolved in CH_2Cl_2 (10.0 ml) inside the glovebox in a volumetric flask. This solution was diluted in a volumetric flask (200 μL in 2.00 ml). The following concentration was present: [(^{t}BuO)$_3$P] = 1 mM, [C_4F_9I] = 1 mM.

S6. Further Computational Details

All line spectra were broadened by Gaussians with standard deviation $\sigma = 1500\ \mathrm{cm}^{-1}$. The isovalue for illustrating the molecular orbitals has been set to 0.05.

S7. Absorption Spectra and Molecular Orbitals

S7.1. Perfluorobutyl Iodide

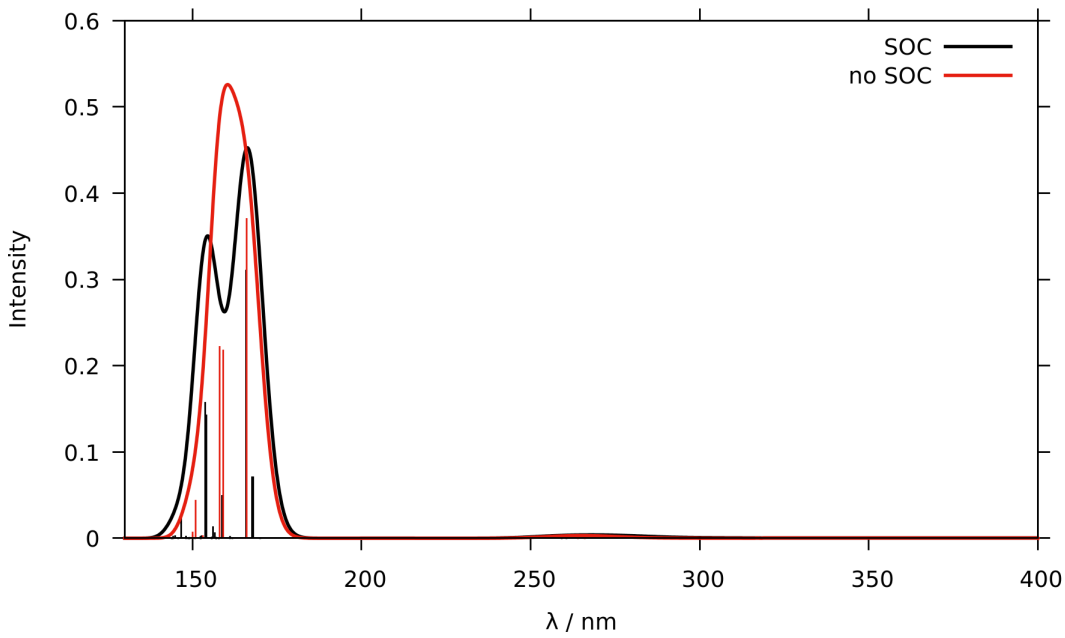

Figure S1. Calculated absorption spectra of C_4F_9I in CH_2Cl_2 with (black) and without (red) spin–orbit coupling (130 – 400 nm).

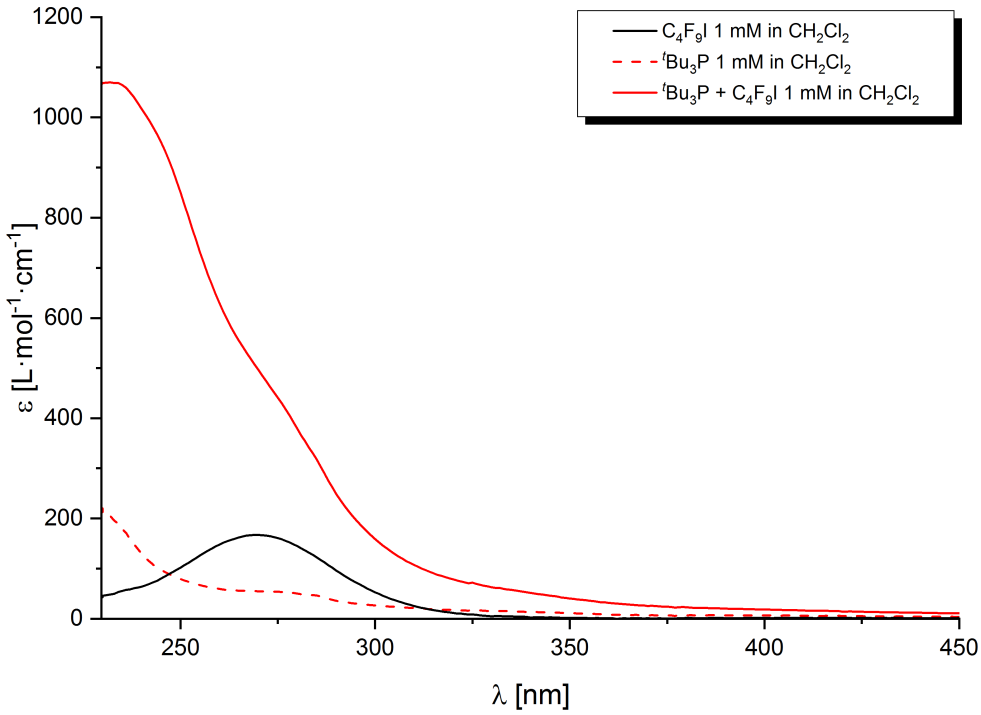

Figure S2. Experimental UV-vis spectra of C_4F_9I (λ_{max} = 270 nm), $^tBu_3P$ (λ_{max} = 227 nm) and $^tBu_3P$ + C_4F_9I (λ_{max} = 232 nm) in CH_2Cl_2.

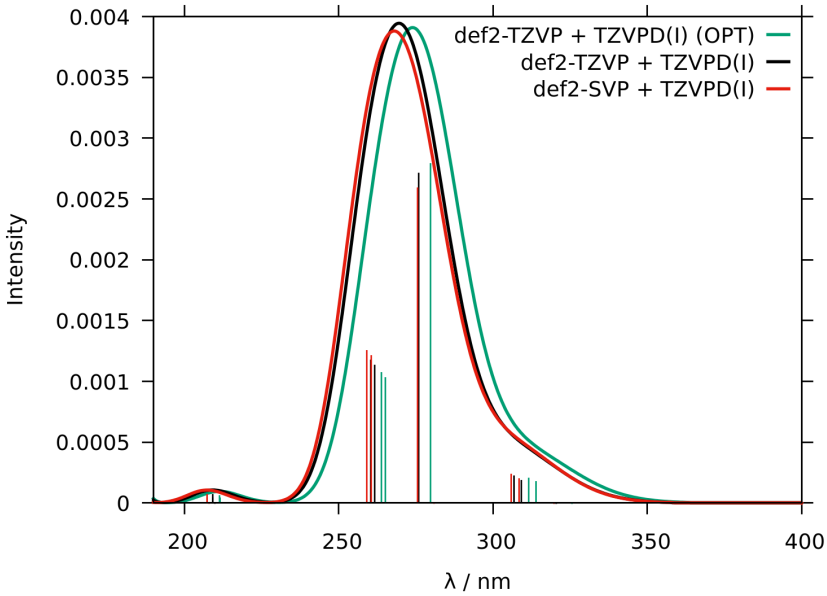

Figure S3. Atomic orbital basis set dependence of the calculated absorption spectrum of C_4F_9I (190 – 400 nm) in CH_2Cl_2 including spin–orbit coupling in quasi-degenerate perturbation theory (DFT/MRCI+SOCQDPT). The red spectrum corresponds to a calculation in the smaller def2-SVP + TZVPD(I) basis set. The black curve, labeled def2-TZVP + TZVPD(I), results from a single-point calculation using the larger def2-TZVP + TZVPD(I) basis set but employing the same geometry parameters as the red one. The green spectrum, labeled def2-TZVP + TZVPD(I) (OPT), was obtained from a set up using the larger def2-TZVP + TZVPD(I) basis set in both, the geometry optimization and DFT/MRCI+SOCQDPT step.

S7.2. Phosphines and Phosphites

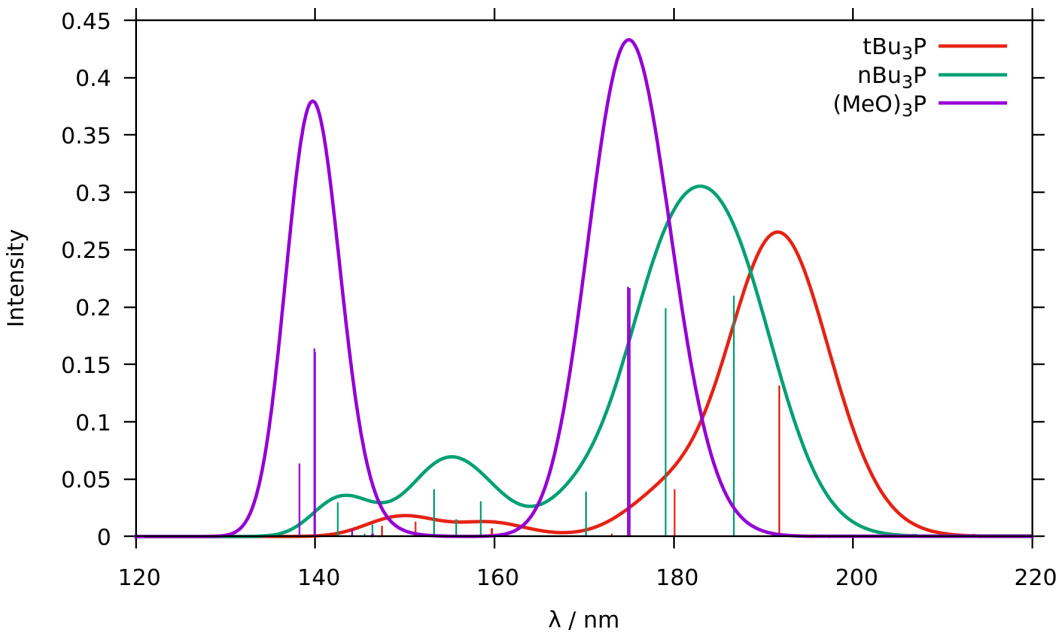

Figure S4. Computed absorption spectra of the phosphines ($^{t}Bu_3P$, $^{n}Bu_3P$) and the phosphite $(MeO)_3P$ in CH_2Cl_2 with spin–orbit coupling (120 – 220 nm).

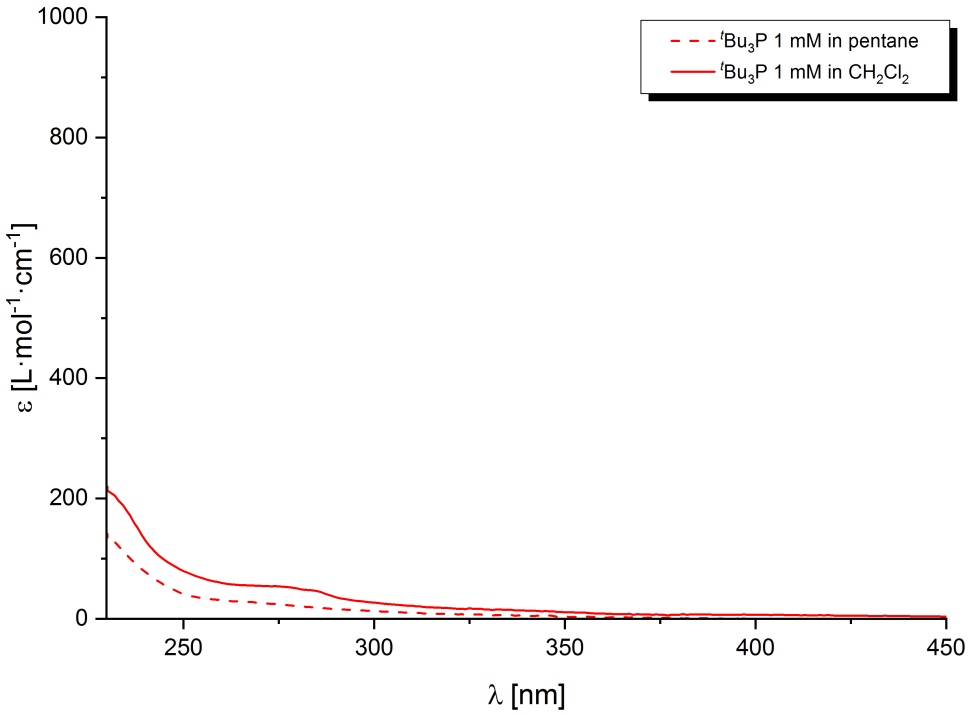

Figure S5. Comparison of the experimental UV-vis spectra of $^{t}Bu_3P$ in pentane (λ_{max} = 227 nm) and in CH_2Cl_2 (λ_{max} = 227 nm).

S7.3. Phosphine and Phosphite Adducts

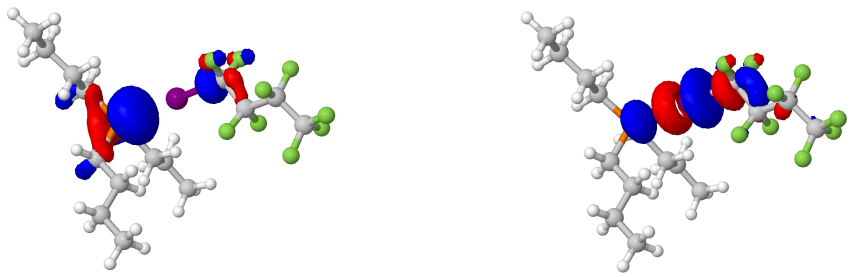

(a) HOMO: n_P (b) LUMO: σ^*

Figure S6. Frontier molecular orbitals of the $^{n}Bu_3P$-IC_4F_9 adduct at the S_0 geometry.

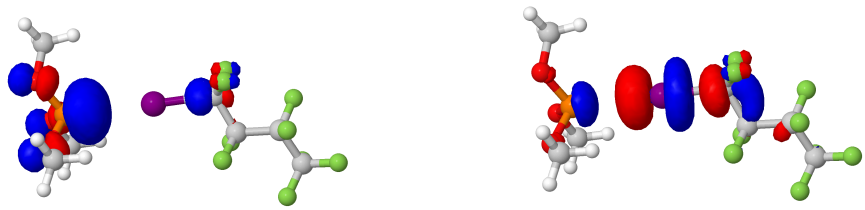

(a) HOMO: n_P (b) LUMO: σ^*

Figure S7. Frontier molecular orbitals of the $(MeO)_3P$-IC_4F_9 adduct at the S_0 geometry.

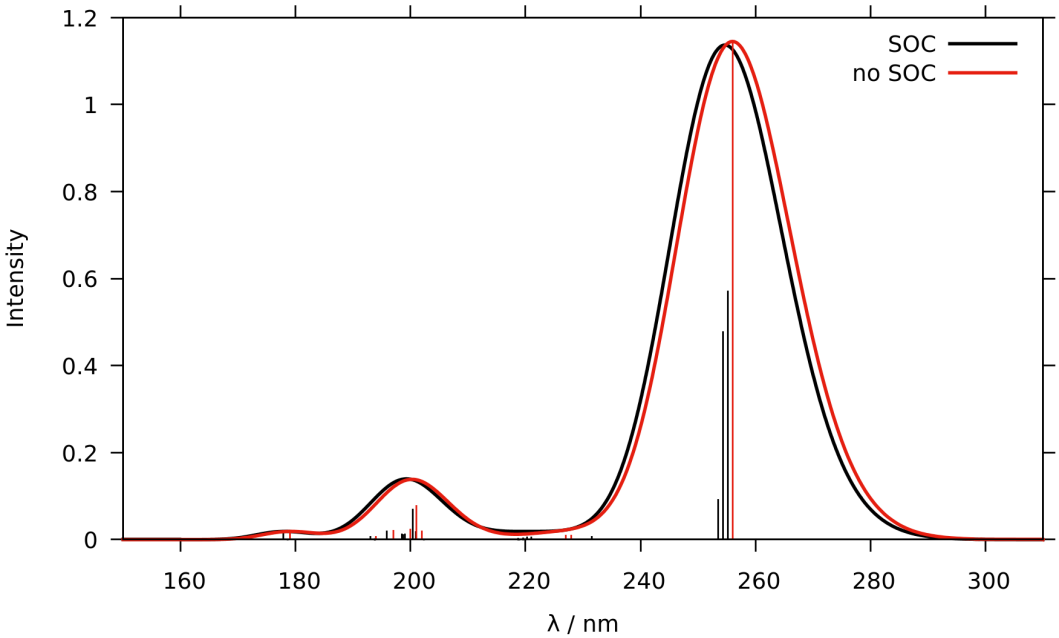

Figure S8. Calculated absorption spectra of $^{t}Bu_3P$–C_4F_9I in CH_2Cl_2 with (black) and without (red) spin–orbit coupling (150 – 310 nm).

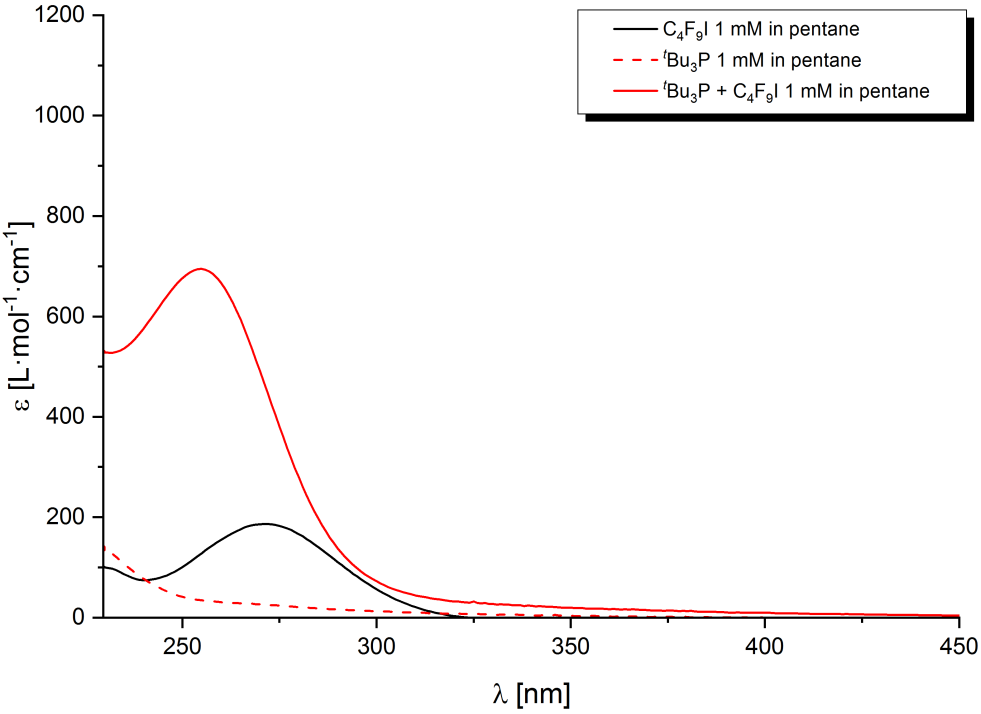

Figure S9. Experimental UV-vis spectra of C_4F_9I (λ_{max} = 270 nm), $^{t}Bu_3P$ (λ_{max} = 227 nm) and $^{t}Bu_3P$ + C_4F_9I (λ_{max} = 255 nm) in pentane.

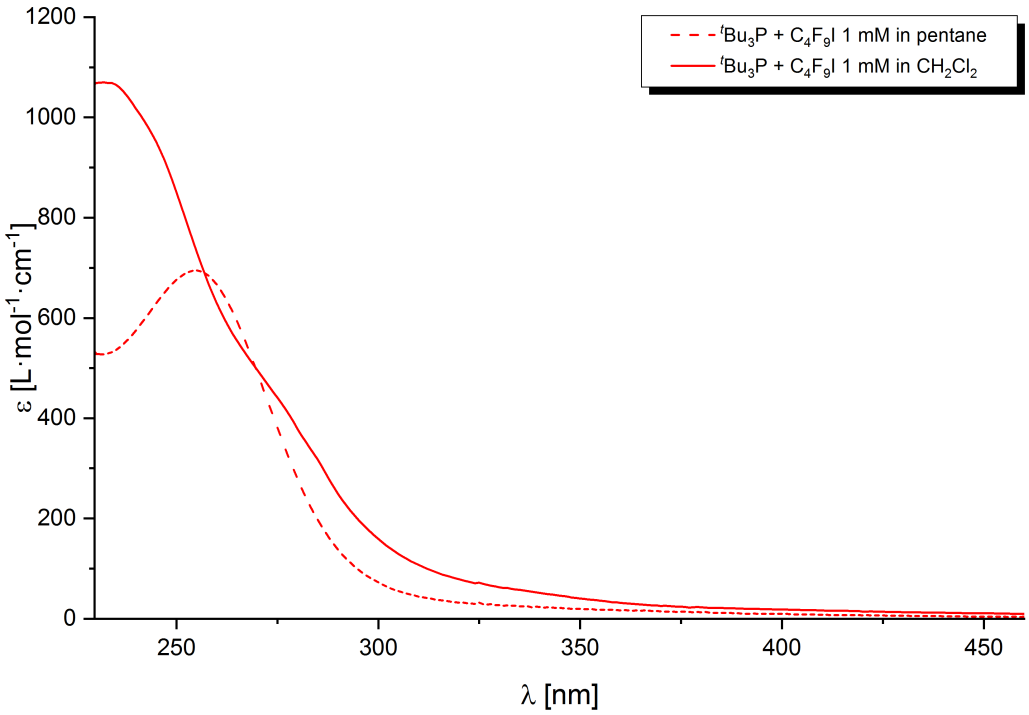

Figure S10. Comparison of the experimental UV-vis spectra of ^{t}Bu$_3$P + C$_4$F$_9$I in pentane (λ_{max} = 255 nm) and in CH$_2$Cl$_2$ (λ_{max} = 232 nm).

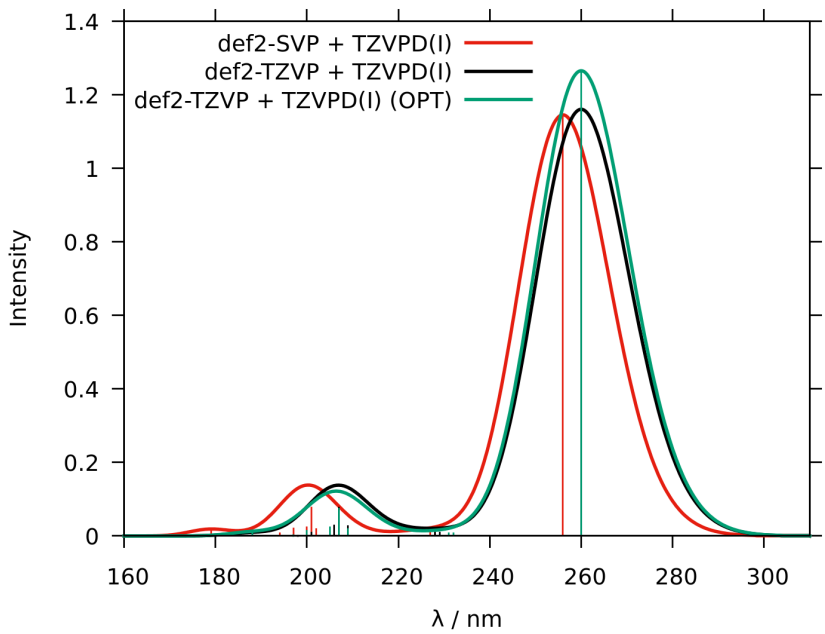

Figure S11. Atomic orbital basis set dependence of the calculated DFT/MRCI singlet absorption spectrum of the ^{t}Bu$_3$P–C$_4$F$_9$I adduct complex (160 – 310 nm). The red spectrum corresponds to a calculation in the smaller def2-SVP + TZVPD(I) basis set. The black curve, labeled def2-TZVP + TZVPD(I), results from a single-point calculation using the larger def2-TZVP + TZVPD(I) basis set but employing the same geometry parameters as the red one. The green spectrum, labeled def2-TZVP + TZVPD(I) (OPT), was obtained from a setup using the larger def2-TZVP + TZVPD(I) basis set in both, the geometry optimization and DFT/MRCI step.

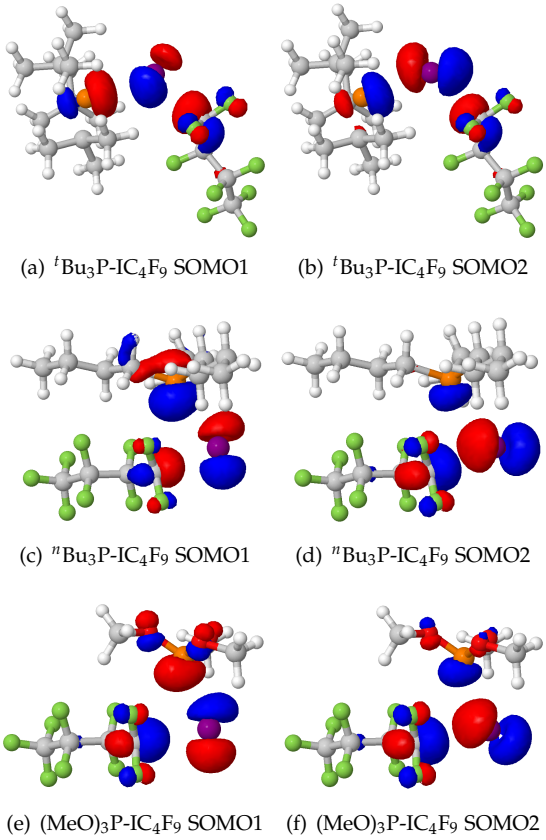

(a) $^{t}Bu_3P$-IC_4F_9 SOMO1 (b) $^{t}Bu_3P$-IC_4F_9 SOMO2

(c) $^{n}Bu_3P$-IC_4F_9 SOMO1 (d) $^{n}Bu_3P$-IC_4F_9 SOMO2

(e) $(MeO)_3P$-IC_4F_9 SOMO1 (f) $(MeO)_3P$-IC_4F_9 SOMO2

Figure S12. Singly occupied MOs (SOMOs) of the phosphine and phosphite adducts in the relaxed T_1 state.

S7.4. Solvent Influence on the Measured Absorption Spectra

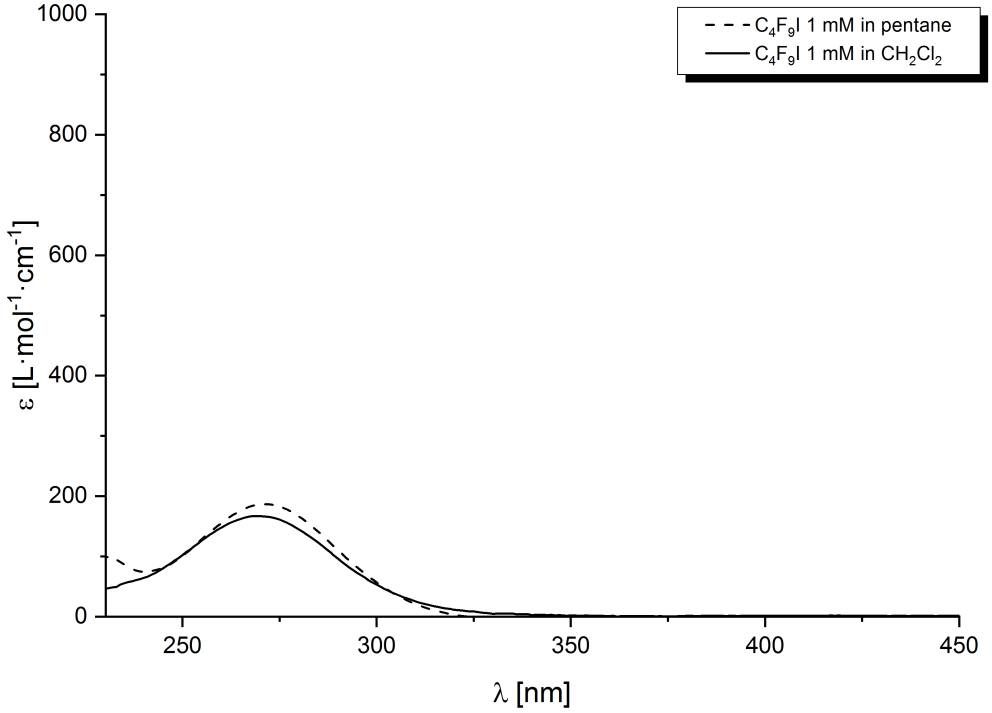

Figure S13. Comparison of the experimental UV-vis spectra of C_4F_9I in pentane (λ_{max} = 270 nm) and in CH_2Cl_2 (λ_{max} = 270 nm).

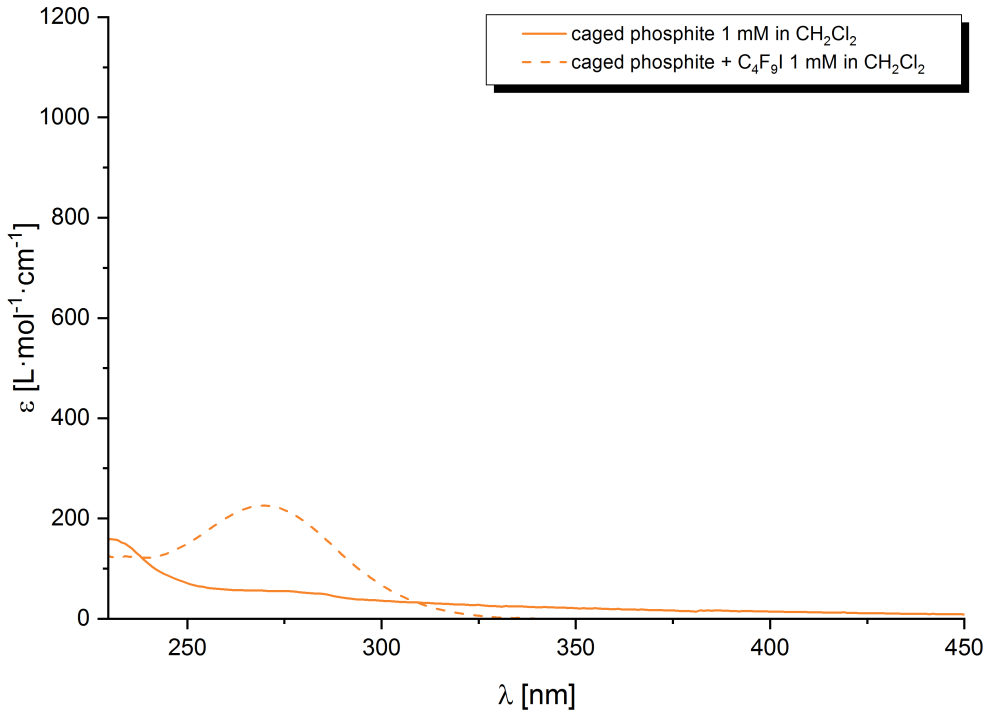

Figure S14. Comparison of the experimental UV-vis spectra of caged phosphite (λ_{max} = 230 nm) and caged phosphite + C_4F_9I (λ_{max} = 270 nm) in CH_2Cl_2.

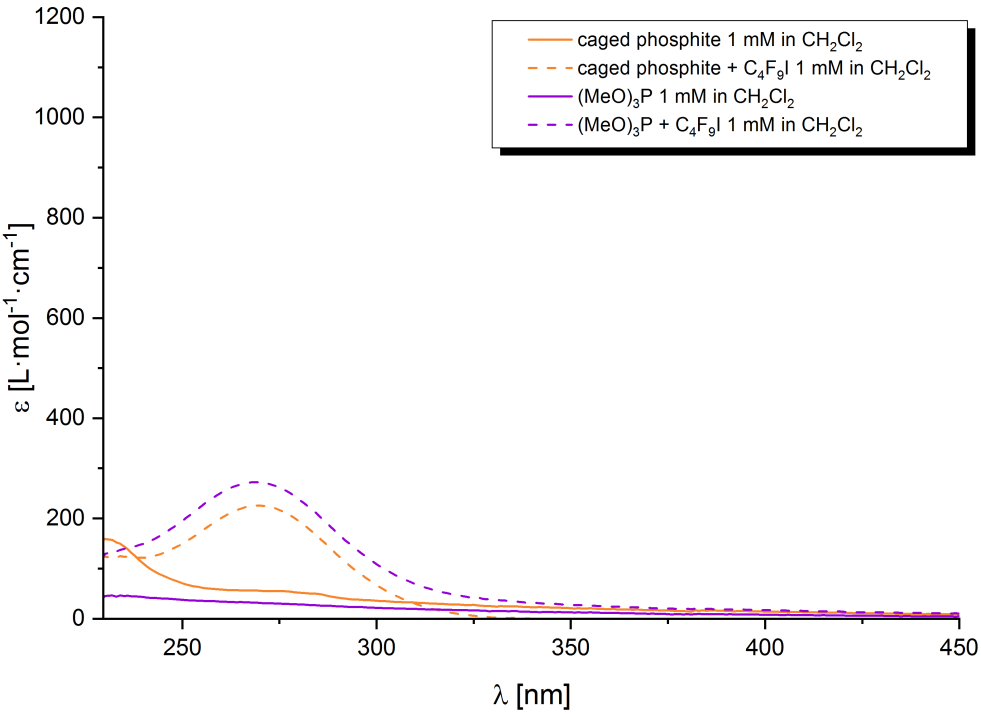

Figure S15. Comparison of the experimental UV-vis spectra of caged phosphite (λ_{max} = 230 nm), caged phosphite + C_4F_9I (λ_{max} = 270 nm), $(MeO)_3P$ ($\lambda_{max} \leq$ 230 nm) and $(MeO)_3P$ + C_4F_9I (λ_{max} = 269 nm) in CH_2Cl_2.

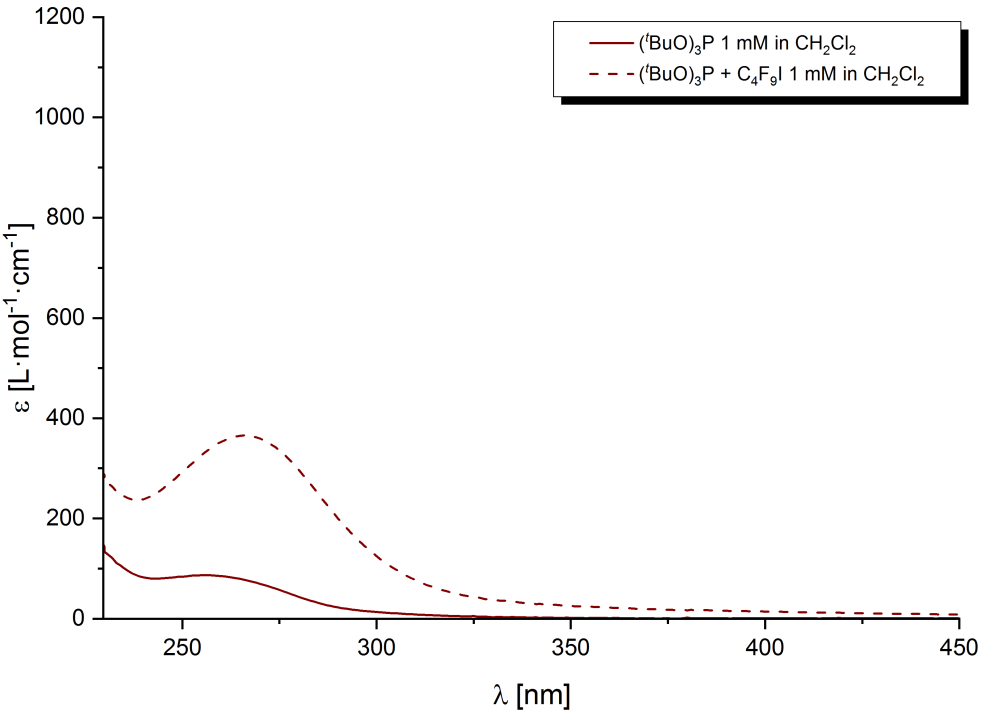

Figure S16. Comparison of the experimental UV-vis spectra of $(^tBuO)_3P$ (λ_{max} = 227 nm) and $(^tBuO)_3P$ + C_4F_9I (λ_{max} = 266 nm) in CH_2Cl_2.

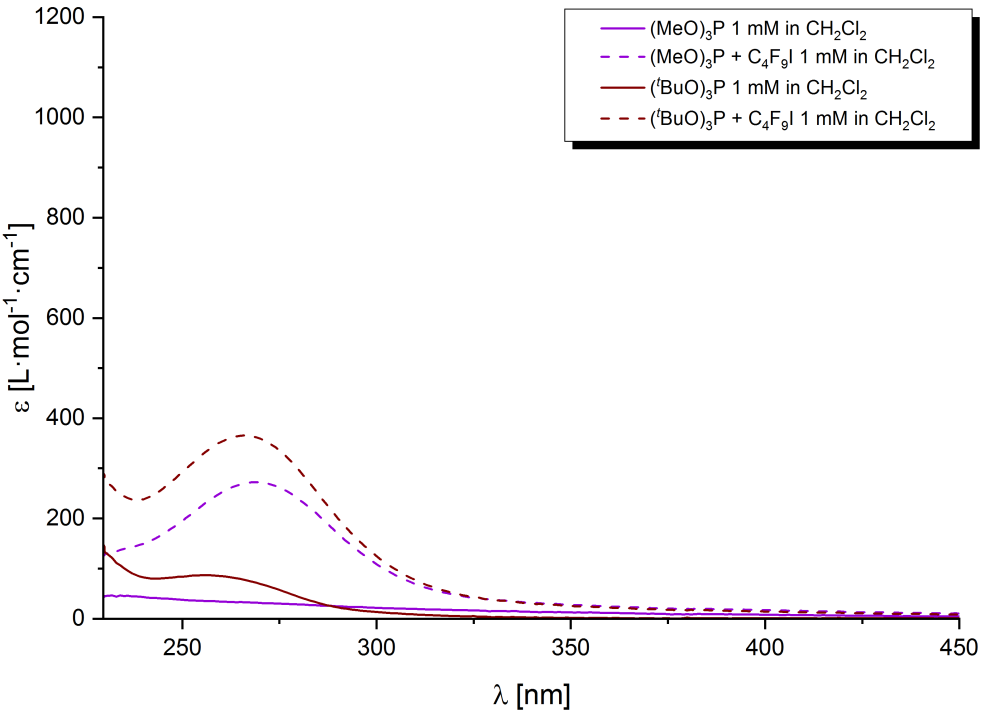

Figure S17. Comparison of the experimental UV-vis spectra of $(MeO)_3P$ ($\lambda_{max} \leq 230$ nm), $(MeO)_3P$ + C_4F_9I (λ_{max} = 269 nm), $(^tBuO)_3P$ (λ_{max} = 227 nm) and $(^tBuO)_3P$ + C_4F_9I (λ_{max} = 266 nm) in CH_2Cl_2.

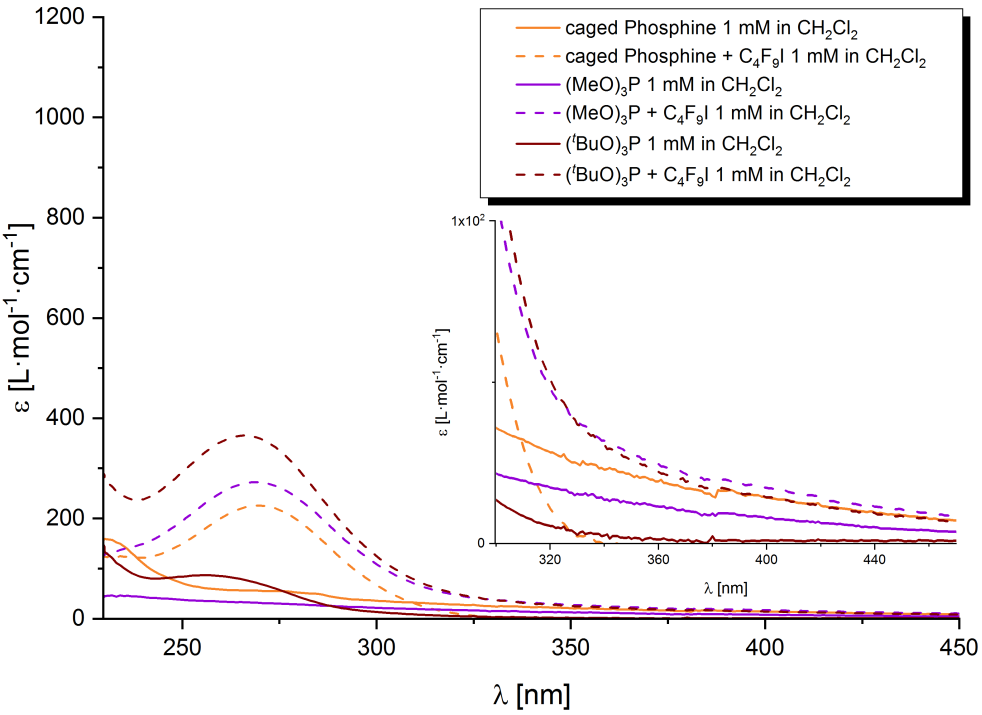

Figure S18. Comparison of the experimental UV-vis spectra of caged phosphite (λ_{max} = 230 nm), caged phosphite + C_4F_9I (λ_{max} = 270 nm), $(MeO)_3P$ ($\lambda_{max} \leq 230$ nm), $(MeO)_3P$ + C_4F_9I (λ_{max} = 269 nm), $(^tBuO)_3P$ (λ_{max} = 227 nm) and $(^tBuO)_3P$ + C_4F_9I (λ_{max} = 266 nm) in CH_2Cl_2.

S7.5. Impact of Spin–Orbit Coupling on the Calculated Spectra

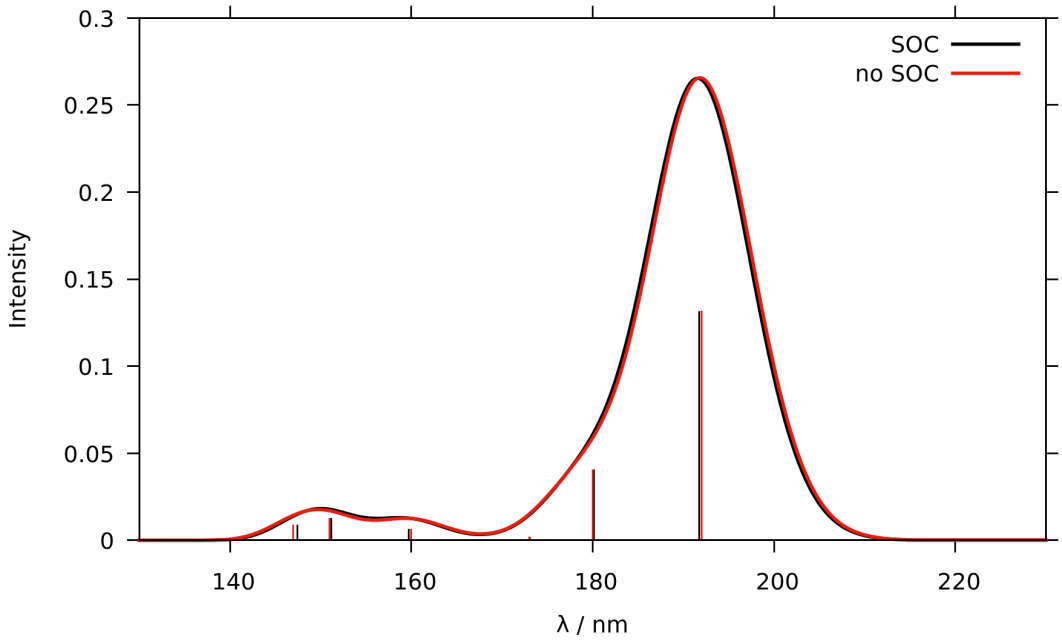

Figure S19. Calculated absorption spectra of $^{t}Bu_3P$ with (black) and without (red) spin–orbit coupling (130 – 230 nm).

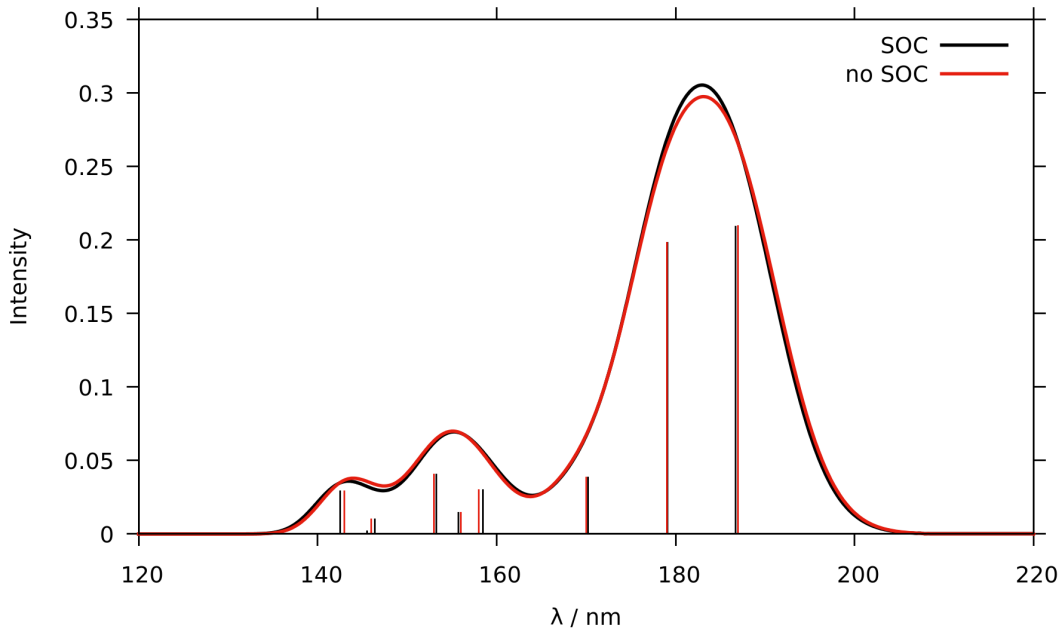

Figure S20. Calculated absorption spectra of $^{n}Bu_3P$ with (black) and without (red) spin–orbit coupling (120 – 220 nm).

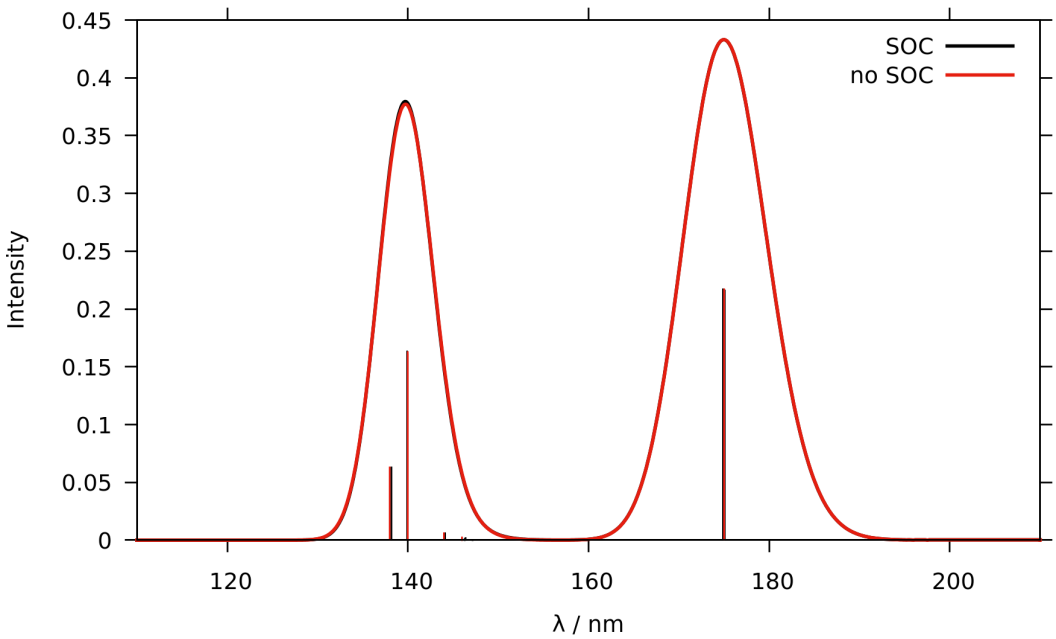

Figure S21. Calculated absorption spectra of $(MeO)_3P$ with (black) and without (red) spin–orbit coupling (110 – 210 nm).

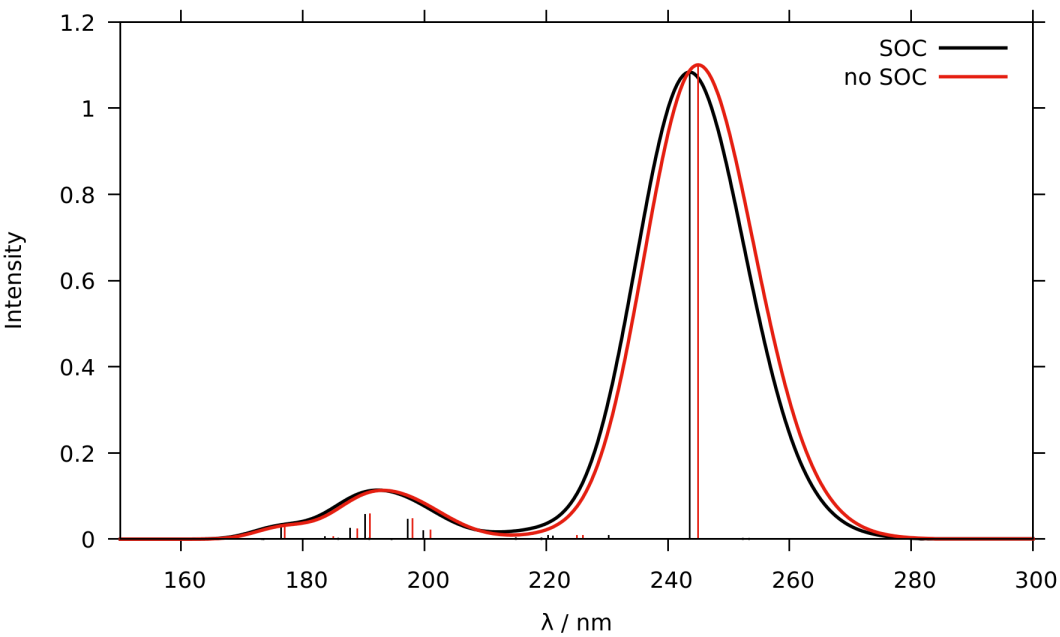

Figure S22. Calculated absorption spectra of $^{n}Bu_3P–C_4F_9I$ with (black) and without (red) spin–orbit coupling (150 – 300 nm).

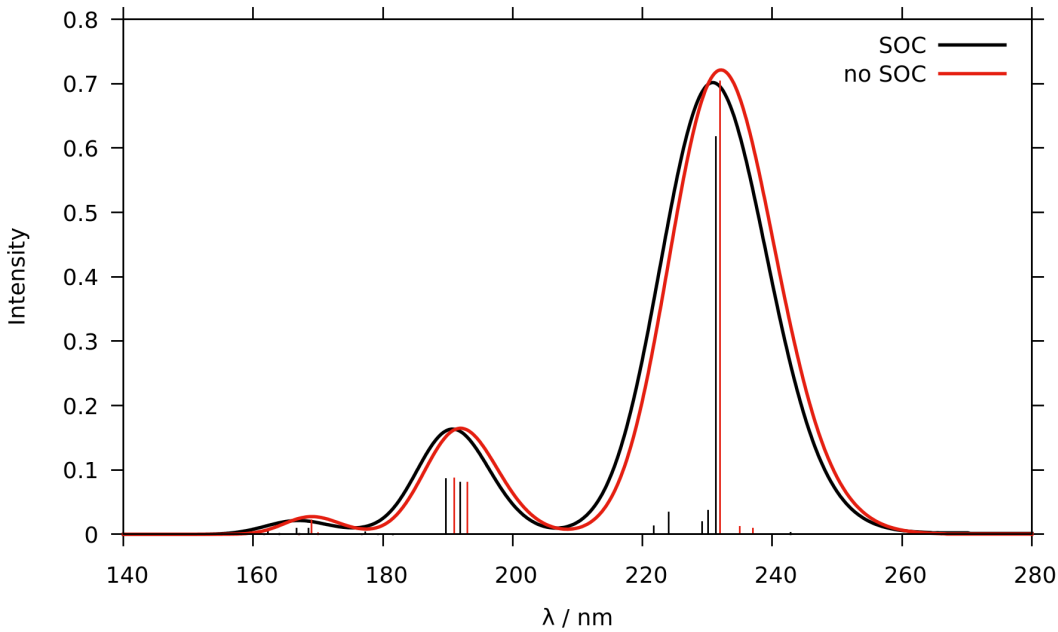

Figure S23. Calculated absorption spectra of $(MeO)_3P–C_4F_9I$ with (black) and without (red) spin–orbit coupling (140 – 280 nm).

S8. Minimum Nuclear Arrangements

S8.1. DFT-Optimized Ground-State Geometries

Perfluoroalkyl Iodide

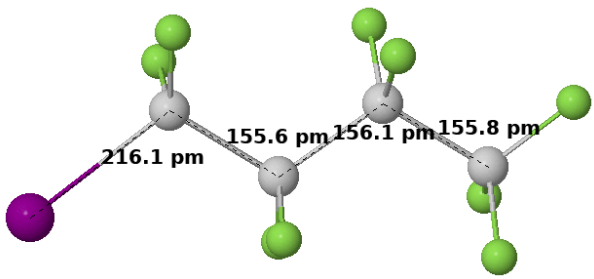

Figure S24. S_0 geometry of C_4F_9I and selected bond lengths in pm.

Phosphines

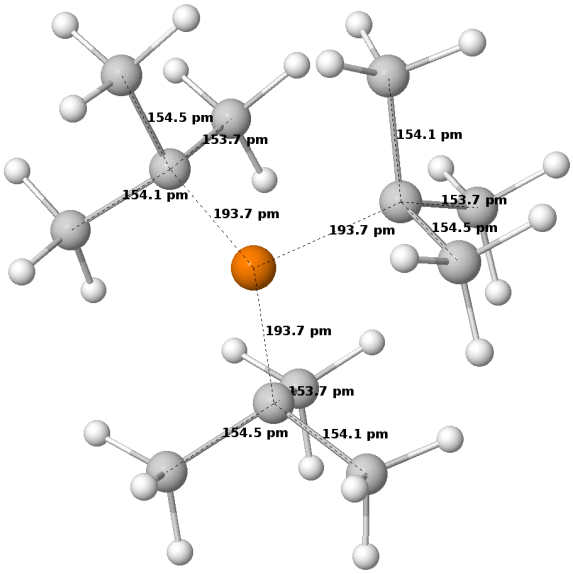

Figure S25. S_0 geometry of $^{t}Bu_3P$ and selected bond lengths in pm.

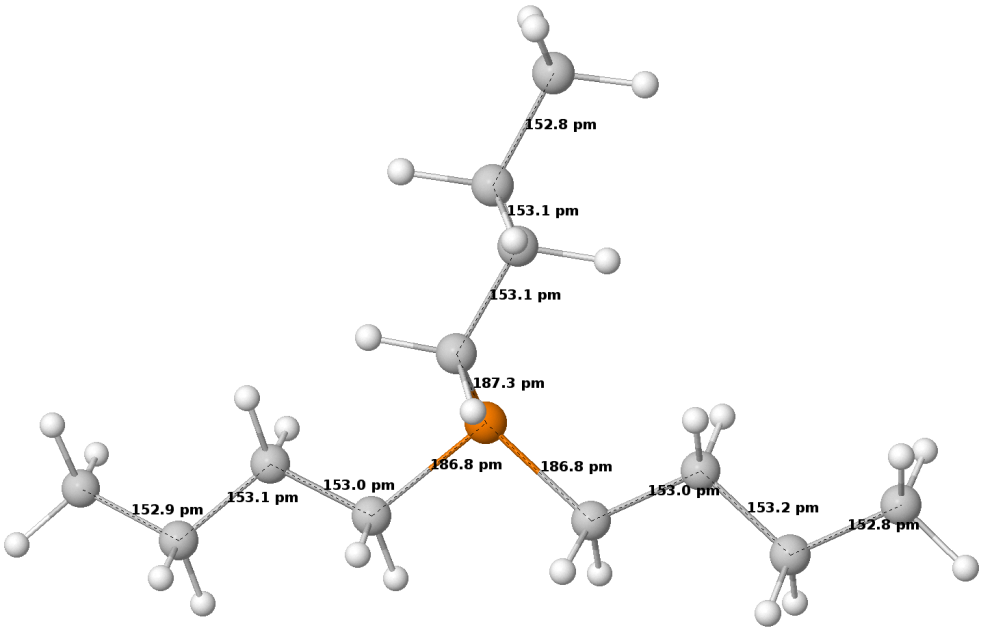

Figure S26. S_0 geometry of $^{n}Bu_3P$ and selected bond lengths in pm.

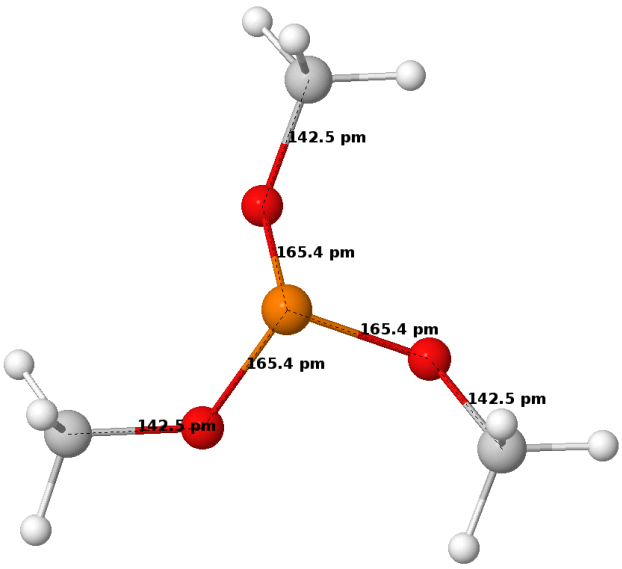

Figure S27. S_0 geometry of $(MeO)_3P$ and selected bond lengths in pm.

Adducts

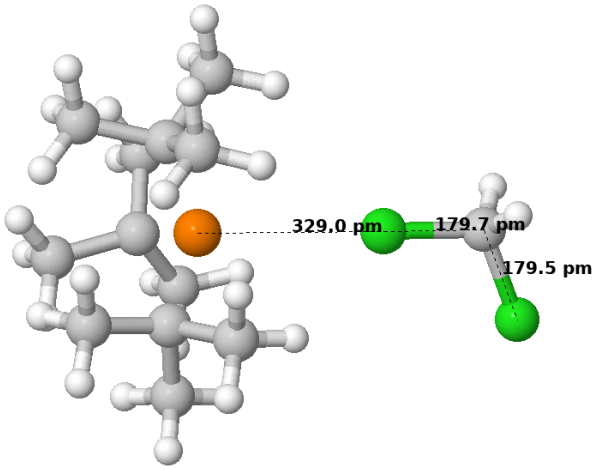

Figure S28. S_0 geometry of $^tBu_3P–CH_2Cl_2$and selected bond lengths in pm.

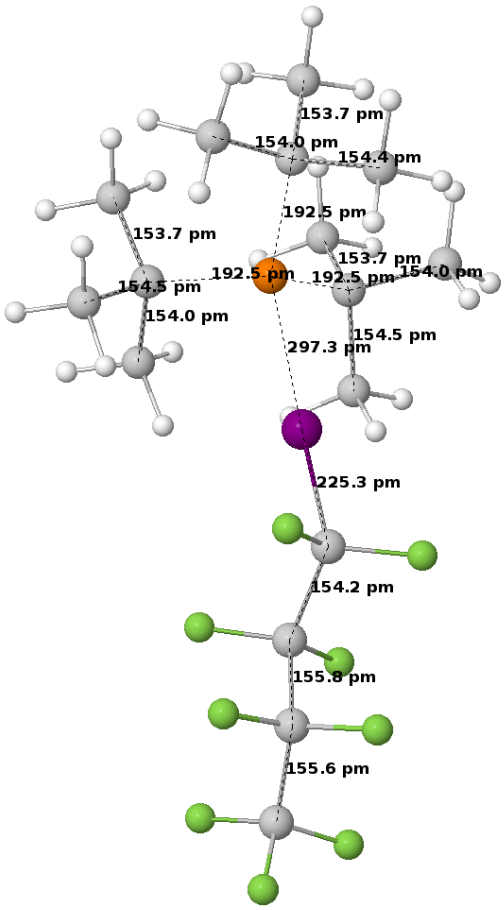

Figure S29. S_0 geometry of ^{t}Bu$_3$P–IC$_4$F$_9$ and selected bond lengths in pm.

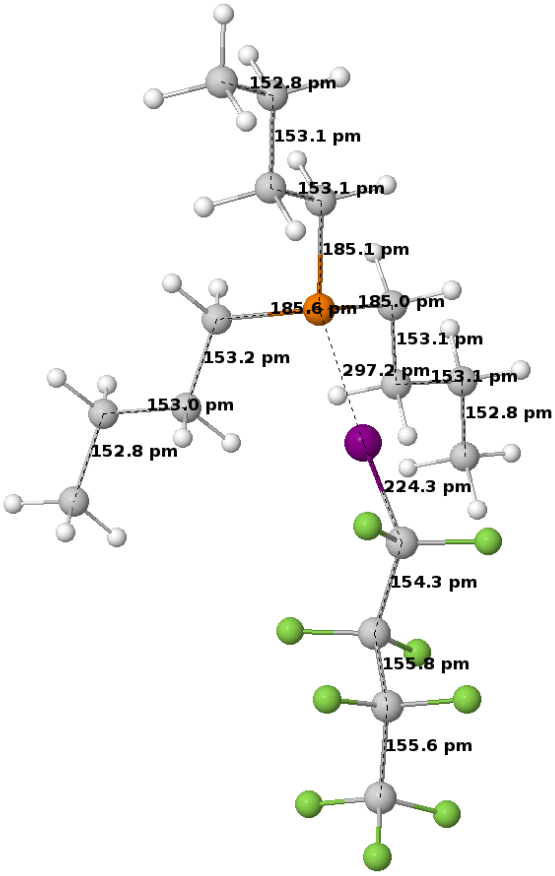

Figure S30. S_0 geometry of ^{n}Bu$_3$P–IC$_4$F$_9$ and selected bond lengths in pm.

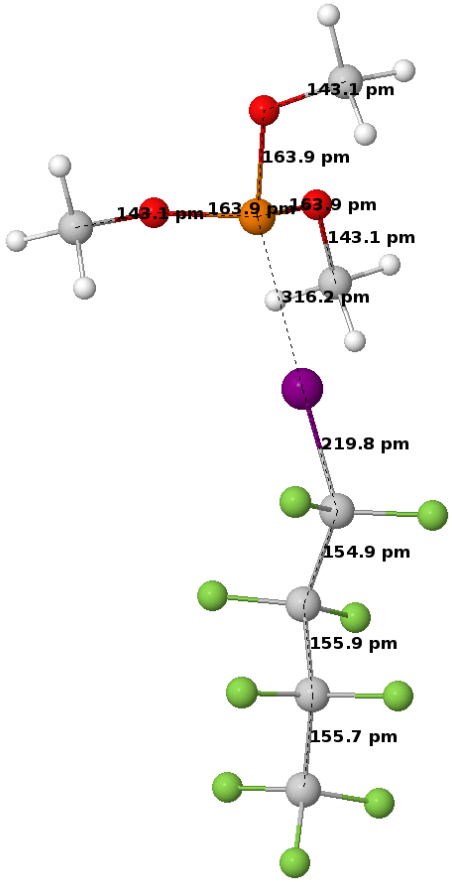

Figure S31. S_0 geometry of $(MeO)_3P–IC_4F_9$ and selected bond lengths in pm.

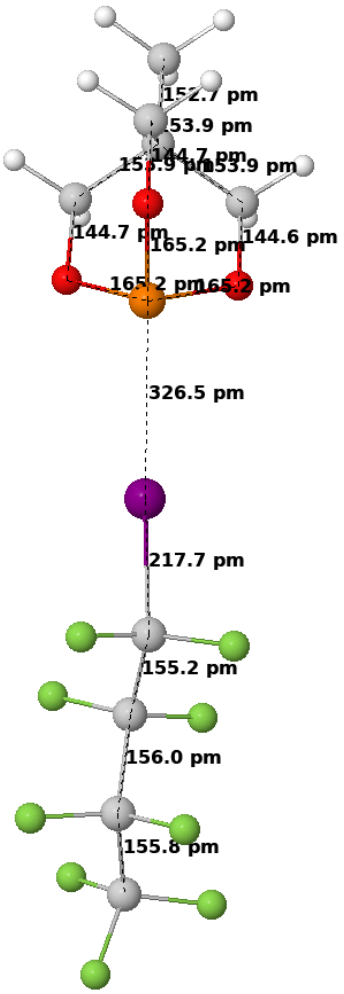

Figure S32. S_0 geometry of the caged phosphite–IC_4F_9 adduct and selected bond lengths in pm.

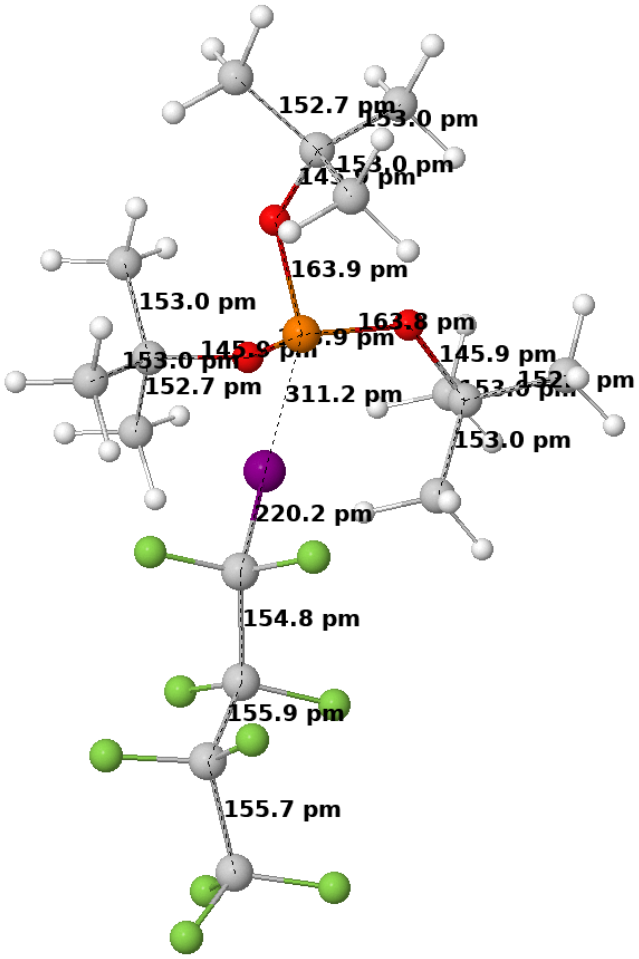

Figure S33. S_0 geometry of $(^t\mathrm{BuO})_3\mathrm{P}–\mathrm{IC}_4\mathrm{F}_9$ and selected bond lengths in pm.

S8.2. TDDFT/TDA-Optimized Conical Intersection Geometries

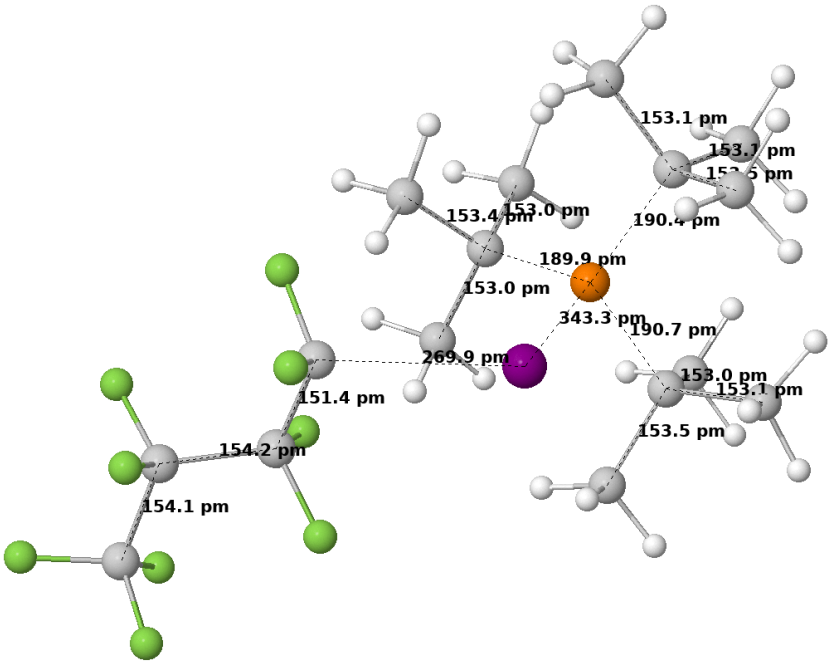

Figure S34. Geometry of the S_1/S_0 conical intersection of ^{t}Bu$_3$P–IC$_4$F$_9$ and selected bond lengths in pm.

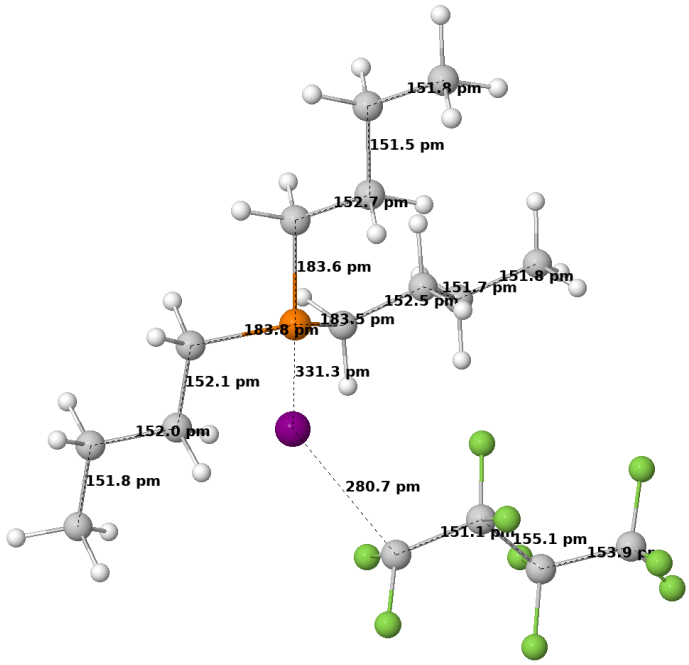

Figure S35. Geometry of the S_1/S_0 conical intersection of ^{n}Bu$_3$P–IC$_4$F$_9$ and selected bond lengths in pm.

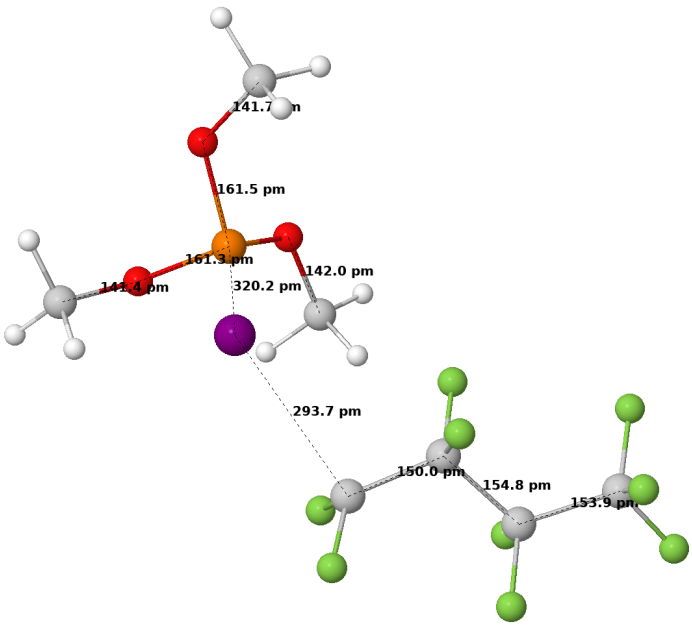

Figure S36. Geometry of the S_1/S_0 conical intersection of $(MeO)_3P–IC_4F_9$ and selected bond lengths in pm.

S8.3. TDDFT/TDA-Optimized Triplet Geometries

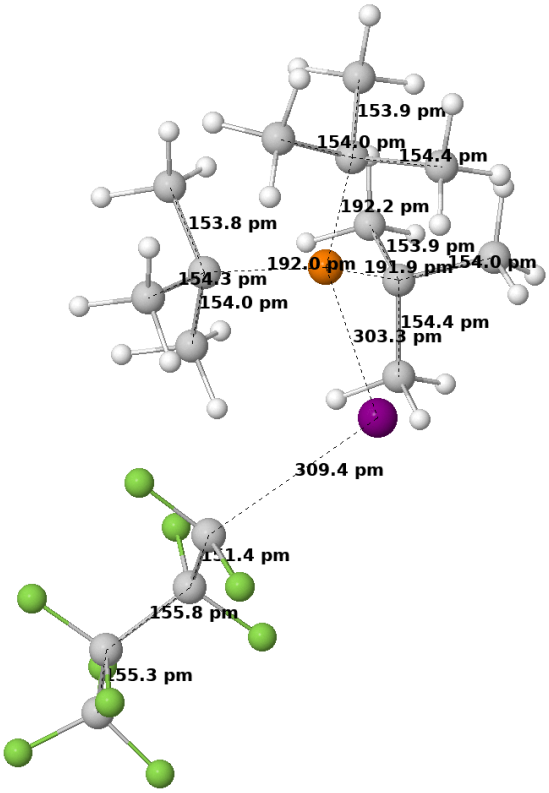

Figure S37. T_1 geometry of $^tBu_3P–IC_4F_9$ and selected bond lengths in pm.

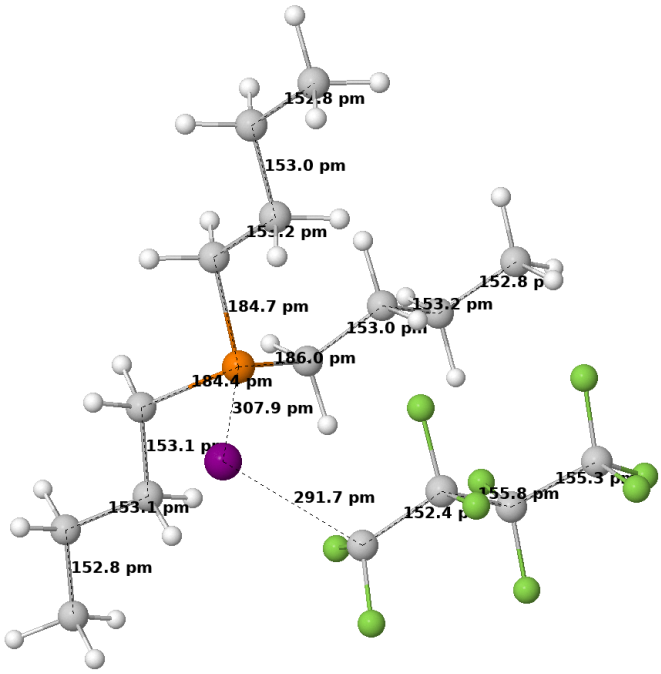

Figure S38. T_1 geometry of ^{n}Bu$_3$P–IC$_4$F$_9$ and selected bond lengths in pm.

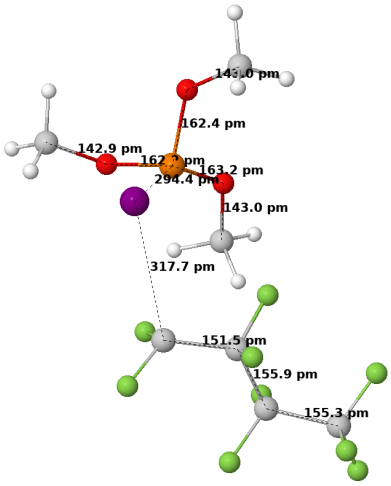

Figure S39. T_1 geometry of (MeO)$_3$P–IC$_4$F$_9$ and selected bond lengths in pm.

1. Helmecke, L.; Spittler, M.; Baumgarten, K.; Czekelius, C. Metal-Free Activation of C–I Bonds and Perfluoroalkylation of Alkenes with Visible Light Using Phosphine Catalysts. *Org. Lett.* **2019**, *21*, 7823–7827. doi:10.1021/acs.orglett.9b02812.
2. Cole, J.R.; Dellinger, M.E.; Johnson, T.J.; Reinecke, B.A.; Pike, R.D.; Pennington, W.T.; Krawiec, M.; Rheingold, A.L. Caged phosphite complexes of copper(I) halides. *J. Chem. Crystallogr.* **2003**, *33*, 341–347. doi:10.1023/A:1024217727932.
3. Taira, K.; Mock, W.L.; Gorenstein, D.G. Experimental Tests of the Stereoelectronic Effect at Phosphorus: Nucleophilic Reactivity of Phosphite Esters. *J. Am. Chem. Soc.* **1984**, *106*, 7831–7835. doi:10.1021/ja00337a029.
4. Manning, H.C.; Bai, M.; Anderson, B.M.; Lisiak, R.; Samuelson, L.E.; Bornhop, D.J. Expeditious synthesis of 'P'-protected macrocycles en route to lanthanide chelate metal complexes. *Tetrahedron Lett.* **2005**, *46*, 4707–4710. doi:10.1016/j.tetlet.2005.05.049.
5. Bietti, M.; Calcagni, A.; Salamone, M. The Role of Structural Effects on the Reactions of Alkoxyl Radicals with Trialkyl and Triaryl Phosphites. A Time-Resolved Kinetic Study. *J. Org. Chem.* **2010**, *75*, 4514–4520. doi:10.1021/jo100703b.
6. Mark, V.; Wazer, J.R.V. Tri-*t*-butyl Phosphite and Some of Its Reactions. *J. Org. Chem.* **1964**, *29*, 1006–1008. doi:10.1021/jo01028a005.